JOURNAL OF GEOPHYSICAL RESEARCH, VOL. 95, NO. B6, PAGES 9343–9370, JUNE 10, 1990

Passive, Off-Axis Convection Through the Southern Flank of the Costa Rica Rift

A. T. FISHER,[1,2] K. BECKER,[1] T. N. NARASIMHAN,[3] M. G. LANGSETH,[4] and M. J. MOTTL[5]

Pore fluids are passively convecting through young oceanic sediments and crust around Deep Sea Drilling Project (DSDP) site 504 on the southern flank of the Costa Rica Rift, as inferred from a variety of geological, geochemical, and geothermal observations. The presence of a fluid circulation system is supported by new data collected on Ocean Drilling Program (ODP) leg 111 and a predrilling survey cruise over the heavily sedimented, 5.9 Ma site; during the latter, elongated heat flow anomalies were mapped subparallel to structural strike, with individual measurements of twice the regional mean value, and strong lateral and vertical geochemical gradients were detected in pore waters squeezed from sediment cores. Also, there is a strong correlation between heat flow, bathymetry, sediment thickness, and inferred fluid velocities up through the sediments. On an earlier DSDP leg, an 8-bar underpressure was measured in the upper 200 m of basement beneath thick sediment cover. Although the forces which drive passive circulation are not well understood, it has generally been thought that the length scale of heat flow variations provides a good indication of the depth of hydrothermal circulation within the oceanic crust. This assumption was based on analytical and numerical analyses of relatively simple porous media models. Deep crustal convection had been inferred near site 504 based on the geometry of surface heat flow anomalies with a wavelength of 4-7 km but appears to be precluded by low crustal permeability, as measured in DSDP hole 504B. The widely varied geothermal and hydrogeological observations near site 504 are readily explained by a model which combines (1) basement relief, (2) irregular sediment drape, (3) largely conductive heat transfer through the sediments overlying the crust, and (4) thermal and geochemical homogenization of pore fluids at the sediment/basement interface, which results from (5) topographically induced, passive hydrothermal circulation with large aspect ratio, convection cells. This convection involves mainly the permeable, upper 200-300 m of crust; the deeper crust is not involved. This convection is induced through a combination of buoyancy fluxes, due to heating from below, and topographic variations on the seafloor and at the basement-sediment interface. This model was designed to incorporate data from both near the sediment surface and deep within boreholes; it is successful in duplicating numerous field observations.

INTRODUCTION: PASSIVE, OFF-AXIS CONVECTION

Hydrothermal convection is not restricted to the crust and sediments immediately adjacent to spreading centers but continues within ridge flanks covered by sediments for tens of millions of years. Evidence supporting this inference includes: off-axis heat flow anomalies [*Williams et al.*, 1974; *Anderson and Hobart*, 1976; *Anderson et al.*, 1977; *Embley et al.*, 1983; *Noel*, 1985; *Langseth et al.*, 1988; *Noel and Hounslow*, 1988], strong lateral and nondiffusive vertical geochemical gradients in sediments [*Maris and Bender*, 1982; *Sayles and Jenkins*, 1982; *Mottl et al.*, 1983*a*; *Leinen et al.* 1983; *Kastner et al.*, 1986], pervasive low-temperature alteration of the chemical and stable isotope compositions of basalts [*Lawrence and Drever*, 1981; *Alt et al.*, 1986], underpressures in shallow basement beneath thick sediment cover [*Hyndman et al.*, 1976; *Anderson and Zoback*, 1982; *Becker et al.*, 1984] which may be dynamically maintained [*Anderson and Zoback*, 1982; *Williams et al.*, 1986], and across-strike variations in the strength of the crustal magnetic field [*Whitmarsh*, 1982].

Lister [1981] labeled this off-axis circulation "passive", as opposed to the "active" circulation commonly seen at spreading centers. Active convection is driven by the tremendous energy released when magma cools and solidifies, during the formation of new oceanic crust. This release of heat creates strong lateral temperature and pressure gradients and may lead to the formation of black smoker, hydrothermal vents. Passive convection takes place on ridge flanks [*Lister*, 1972, 1981] where heat flow is generally less than several hundred milliwatts per square meter beneath crust older than several million years [*Parsons and Sclater*, 1977]. Although less vigorous than its axial counterpart, off-axis circulation may comprise >80% of the total seawater flux through oceanic crust [*Morton and Sleep*, 1985; *Fehn and Cathles*, 1986]. The mechanics of off-axis circulation may be relatively easy to describe, in comparison to axial convection. For example, changes in the physical properties of sediments and basalt, resulting from high-temperature fluid flow and the precipitation of hydrothermal minerals near the ridge crest [*Fyfe and Lonsdale*, 1981], have probably slowed in off-axis areas, where fluid temperatures and velocities are lower [*Lister*, 1981]. In addition, the sediments deposited on ridge flanks may inhibit fluid communication between underlying crust and the overlying ocean [*Anderson and Hobart*, 1976; *Anderson et al.*, 1977; *Karato and Becker*, 1983]. Finally, while there has been broad speculation as to the importance of multiphase flow in black smoker hydrothermal systems at spreading centers [*Bischoff and Rosenbauer*, 1984, 1985; *Goldfarb and Delaney*, 1988; *Cowan and Cann*, 1988], single-phase flow is probably the rule in most off-axis areas where

[1]Division of Marine Geology and Geophysics, Rosenstiel School of Marine and Atmospheric Science, University of Miami, Florida.

[2]Now at Ocean Drilling Program, Texas A & M University, College Station.

[3]Earth Sciences Division, Lawrence Berkeley Laboratory, Berkeley, California.

[4]Oceanography, Lamont-Doherty Geological Observatory, Palisades, New York.

[5]Department of Oceanography, University of Hawaii and Hawaii Institute of Geophysics, Honolulu.

Paper number 89JB01500.
0148-0227/90/89JB-01500$05.00

high pressures and low temperatures keep fluid properties well below the critical point.

However, the plumbing of off-axis as well as on-axis convection systems is still not well understood. We do not know how deeply fluids circulate into the crust, how long circulation continues, nor what mechanisms actually end hydrothermal activity in older crust. Fluid flow velocities and the typical degree of crust/sediment/seawater interaction are also unknown. Finally, it is not obvious how vertical and lateral heterogeneities and anisotropy alter convection geometry and intensity.

This study summarizes results from recent oceanographic and drilling expeditions to the southern flank of the Costa Rica Rift and presents analytical analyses and numerical simulations which use these data to constrain conceptual models of passive circulation. Field data are reviewed, along with the origin of surface heat flow anomalies, the possibility of whole crustal convection, and evidence for fluid flow through the sediments and crust at low velocities. A combination of geothermal and geochemical data provide compelling arguments for the existence of off-axis convection at site 504, although it is not clear from the field data alone how such a system is driven and maintained. A two-dimensional numerical model of the area around site 504 appears to explain reasonably many observations, including underpressures in the upper few hundred meters of basement [*Anderson and Zoback*, 1982], pore fluids which flow vertically and laterally through thick sediments [*Langseth and Mottl*, 1982; *Mottl et al.*, 1983*a*; *Mottl*, 1989] and the apparent correlation between heat flow, bathymetry, fluid velocities, and sediment thickness [*Langseth et al.*, 1988; *Mottl*, 1989].

A BRIEF REVIEW OF FIELD STUDIES

Geological and Geophysical Setting on the Southern Flank of the Costa Rica Rift

The Costa Rica Rift (CRR) is the eastern-most segment of the Galapagos Spreading Center (GSC) complex [*Lonsdale*, 1977; *Lonsdale and Klitgord*,1978; *Costa Rica Rift United Scientific Team (CRRUST)*, 1982], running from 83°00'W to 84°30'W, near the center of the Panama Basin at 3°10'N (Figure 1). Deep Sea Drilling Project (DSDP) site 504 is located half way between the Panama and Ecuador fracture zones, about 200 km south of the spreading axis. Sedimentation under the eastern equatorial productivity zone at site 504 is about 40-60 m m.y.$^{-1}$ [*Sancetta*, 1983], somewhat higher than usual over a mid-ocean ridge. The smooth, heavily sedimented seafloor south of the GSC may have been effectively sealed from hydrothermal exchange when sediment thickness reached 50-200 m, after perhaps 1-4 m.y. [*Anderson and Hobart;* 1976; *Karato and Becker*, 1983].

Basement relief on the southern flank of the CRR is primarily along normal faults that strike east to west, parallel to the rift and to magnetic lineations in the crust [*Langseth et al.*, 1983]. These faults separate downdropped grabens, typically tilted to the south, and ridges which are 1-2 km wide [*Hobart et al.*, 1985]. Sea floor bathymetry is fairly smooth with variations of ±60 m; sediments are thicker in bathymetric and basement troughs and thinner over ridges (Figures 2 and 3). Near DSDP site 504, upper crustal velocities are higher and shear wave arrivals somewhat stronger than usual [*CRRUST*, 1982], possibly due to the sealing of cracks and pores in the upper basalt after thick sediments isolated the crust from the overlying ocean [Langseth et al., 1983]. A detailed seismic survey over the site [*Brocher et al.*, 1986] apparently revealed reflectors at the top of seismic layer 2 (5 s two-way travel time), at the top of seismic layer 3 (5.3 s) about 150 m below the present bottom of hole 504B, and a discontinuous reflector (1.6 s below basement) which may be a low-velocity zone near the Moho.

Heat Flow Studies

DSDP sites 504 and 505 (Figure 1) were chosen as a two-site transect to examine geothermal processes in young, heavily sedimented crust [*Langseth et al.*, 1983; *Hobart et al.*, 1985; *Becker et al.*, 1989]. Highly scattered heat flow near site 505 averages 10-20% of that predicted for 3.9 Ma crust [*Anderson and Hobart*, 1976; *Langseth et al.*, 1983]. Extensive basement outcropping, due to rough bathymetry and incomplete sediment cover, and irregular surface heat flow combined with linear thermal gradients in the upper sediments suggest that fluid convection through faults and outcrops is removing much of the crustal heat at site 505 [*Hobart et al.*, 1985].

Near site 504, sediments are thicker, bathymetry is smoother, and heat flow fluctuates about the value predicted for crust of 5.9 Ma,194 mW m^{-2} [*Parsons and Sclater*, 1977; *Langseth et al.*, 1983; *Hobart et al.*, 1985; *Langseth et al.*, 1988]. The area between sites 505 and 504 appears to be one of thermal transition from a convective to a conductive regime (Figure 4) [*Langseth et al.*, 1983]. The mean surface heat flow around site 504 is 218 ±36 (s.d.) mW m^{-2}, with individual values ranging from 166 to 395 mW m^{-2} (Figures 5 and 6). Variations in heat flow are located in

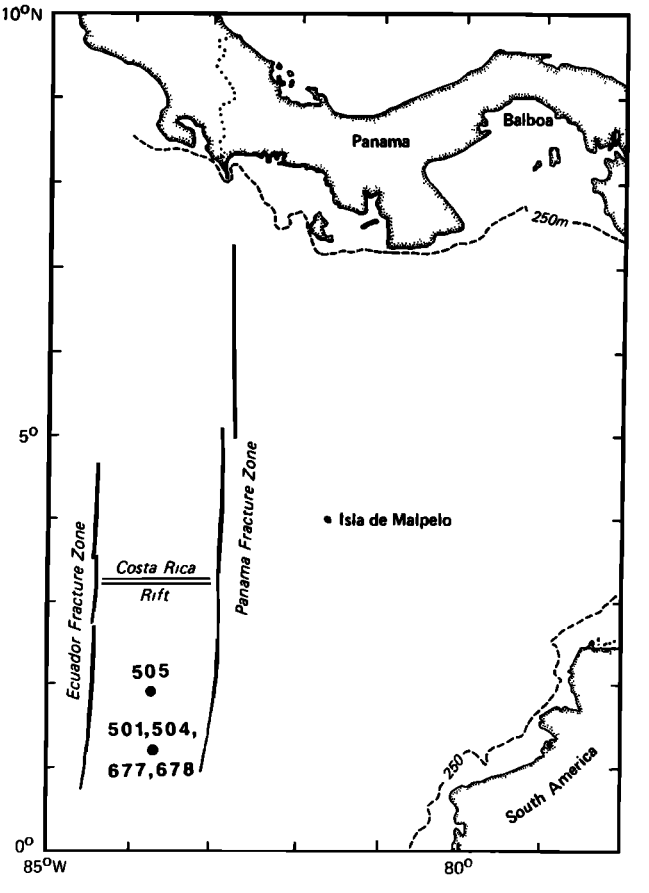

Fig. 1. DSDP/ODP sites 504, 505, 677, and 678 on the southern flank of the Costa Rica Rift, in the eastern equatorial Pacific.

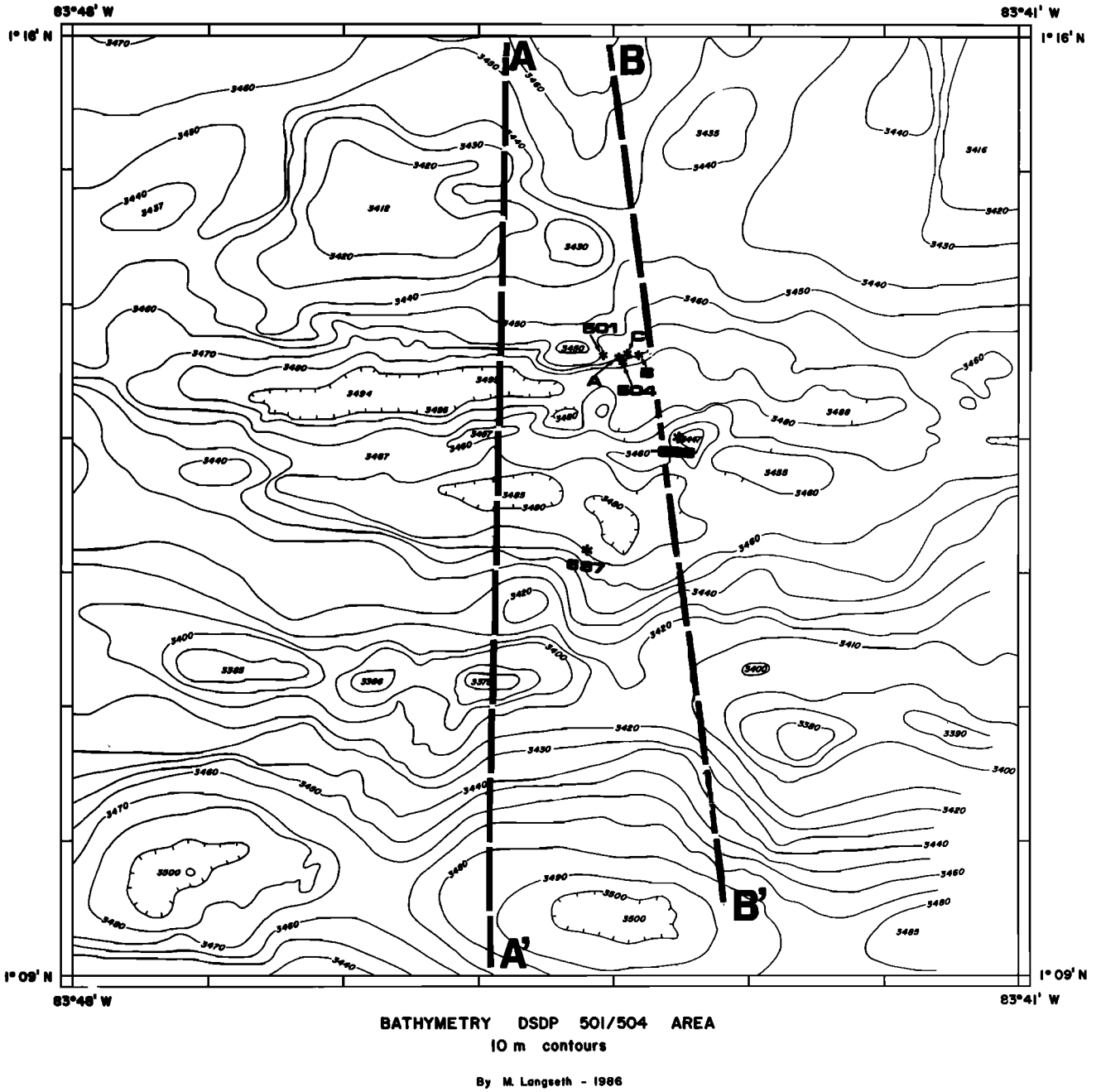

Fig. 2. Contour map of bathymetry near DSDP site 504 determined from GPS- and transponder-navigated echo soundings. Locations of DSDP holes 501 and 504A-C and ODP sites 677 and 678 and positions of seismic lines A-A' and B-B' are also shown [*Langseth et al.*, 1988]. The region shown has dimensions of 13 km on a side.

narrow "warm spots" over basement and bathymetric ridges, and lower values cover larger areas in troughs (Figures 2 and 6). The wavelength of heat flow variations is, like bathymetry, of the order of 4-7 km; warm and cool zones generally strike east to west, subparallel to the distant ridge crest and local topography. Thermal conductivity is relatively consistent laterally and with depth in the upper 9 m of sediment, averaging 0.73-0.80 W m^{-1} K^{-1} [*Langseth et al.*, 1988]. Thermal gradients measured in the upper 2-8 m of sediments were uniformally linear, indicating no fluid flow at velocities greater than about $10^{-8.5}$ m s^{-1}, or 100 mm yr^{-1}, the minimum detectable with a 5-m probe and background heat flow of 200 mW m^{-2} [*Langseth and Herman*, 1981; *Fisher*, 1989].

Geothermal Results From DSDP Hole 504B

Downhole temperatures have been measured 13 times at site 504, including one profile of sediment temperatures in hole 504C and 12 open-hole logs in hole 504B [*Becker et al.*, 1983*a*,*b*, 1985, 1988; *Gable et al.*, 1989]. Four open-hole profiles were measured under "equilibrium" conditions, immediately after reentry following long time periods of inactivity (Figure 7). Sediment temperatures in hole 504C indicate conductive heat flow of about 196 mW m^{-2}, suggesting that the temperature at the sediment/basement contact is about 58°C [*Becker et al.*, 1983*a*].

In contrast, temperatures measured in the upper 400 m of hole 504B (cased through sediment and open in basement) reflected the

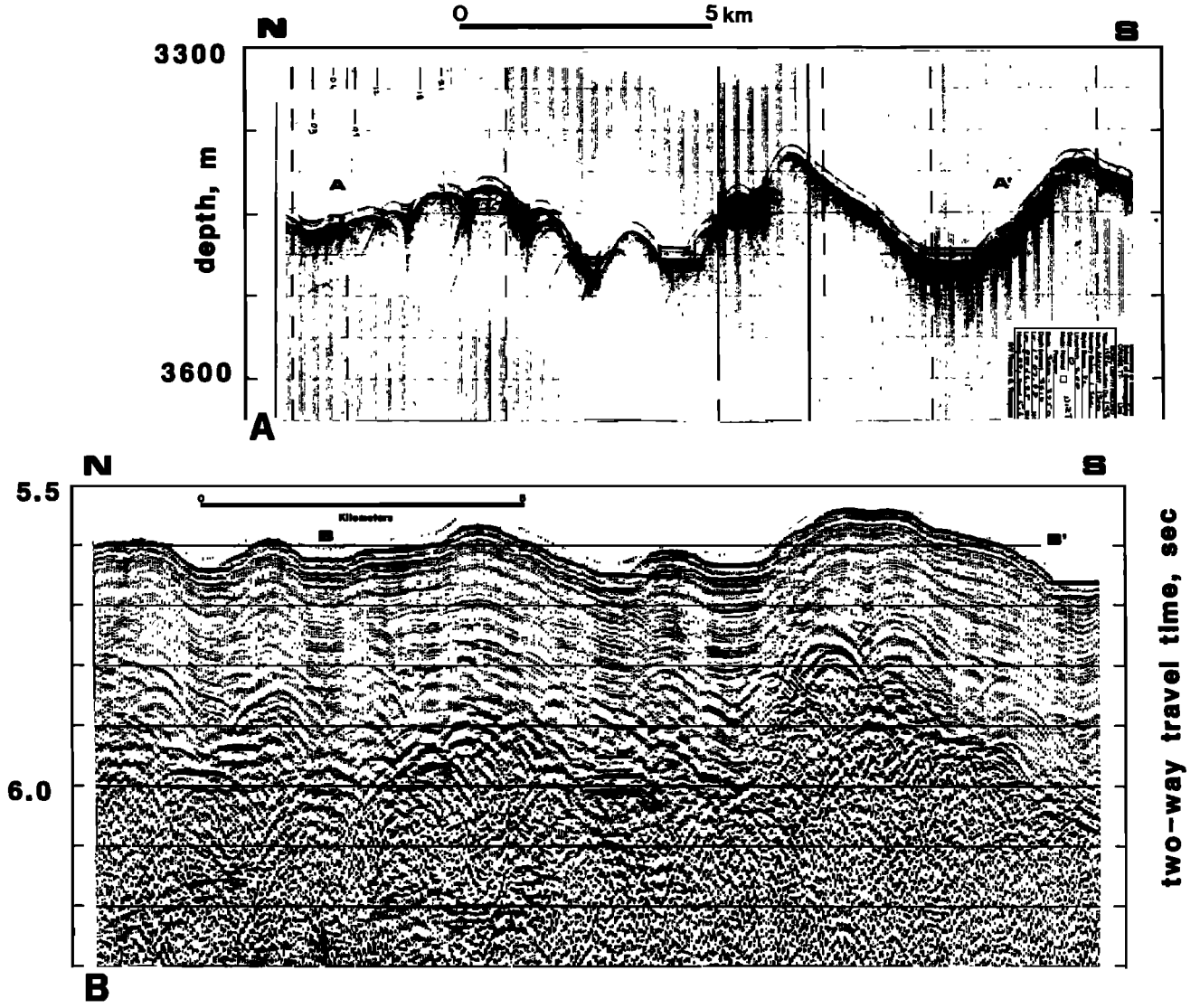

Fig. 3. (*a*) Reproduction of 3.5 kHz record along line A-A' (Figure 2). Depths computed assuming acoustic velocity 1500 m s^{-1} in water. (*b*) SCS section along line B-B' (Figure 2). Processing parameters: pass filter 30-220 Hz, time-varying gain [Langseth et al.,1988].

draw down of cold ocean bottom water into underpressured and relatively permeable pillow lavas in the upper 100 m of the crust [*Anderson and Zoback*, 1982; *Becker et al.*, 1983*a*,*b*] (Figure 7b). *Anderson and Zoback* [1982] measured an underpressure of about 8 bars (8×10^5 Pa) in the upper 200 m of basement. *Becker et al.* [1983*a*] demonstrated that the initial fluid flow velocity was about 90 m yr^{-1} (7000 L hr^{-1}) when hole 504B was drilled, but this flux was reduced by over 99% when the hole was reoccupied 7 yr later on Ocean Drilling Program (ODP) leg 111 [*Becker et al.*, 1988; *Gable et al.*, 1989]. DSDP Holes 335 and 395A in young Atlantic crust experienced a similar fluid draw down after penetration of a sediment cap overlying basement [*Hyndman et al.*, 1976; *Becker et al.*, 1984]. *Anderson and Zoback* [1982] suggested that the underpressure in the upper oceanic crust around hole 504B required a dynamic source, because a static underpressure would decay within a few hundred thousand years after formation.

Packer measurements suggest that the only significantly permeable zone around hole 504B is in the uppermost 200 m of pillow lavas, where the permeability was determined to average 10^{-14} to 10^{-13} m^2 [*Anderson and Zoback*, 1982]. *Anderson et al.* [1985] and *Becker* [1989] measured an average permeability around 10^{-17} m^2 in the lower kilometer of the hole.

Pore Water Geochemistry

Pronounced vertical and lateral gradients in Ca^{++}, Mg^{++} and alkalinity in sediment pore fluids recovered on DSDP leg 69 suggested that either (1) basement pore waters varied laterally in composition, or (2) sediment pore water composition was strongly affected by nonuniform lateral advection and/or diffusion [*Mottl et al.*, 1983 *a*]. Piston cores collected around site 504 in 1982 revealed no detectable vertical pore water chemical gradients in low heat flow areas, and small but measurable gradients in calcium and magnesium where heat flow was >225 mW m^{-2} [*Langseth and Mottl*, 1982]. Fifteen cores collected in 1986, some of which originated in heat flow highs, revealed a wider range in vertical and lateral geochemical gradients [*Langseth et al.*, 1988]. There was a definite positive mole-by-mole correlation between Ca^{++} and Mg^{++} in the sediment pore waters from cores, as is generally attributed to basalt alteration in basement [*Lawrence et*

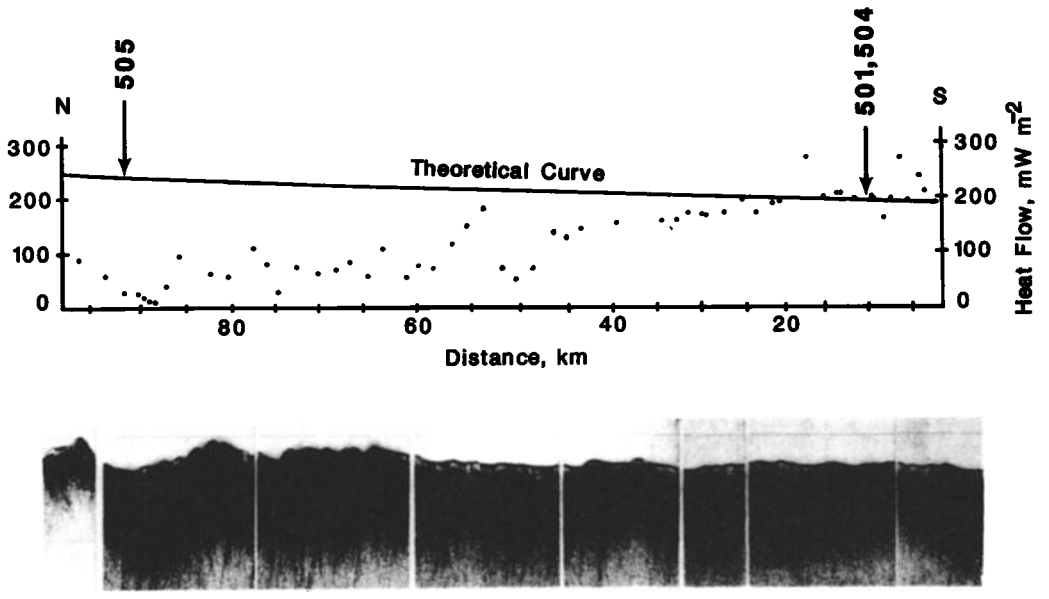

Fig. 4. Heat flow versus distance (age) in a north-south line covering DSDP sites 505 and 504, displayed over a single-channel seismic reflection profile showing basement topography and an increase in sediment thickness with age [*Langseth et al.*, 1983; *Hobart et al.*, 1985] (also previously unpublished data from cruise TT-198).

al., 1975; *Lawrence and Gieskes*, 1981]. In one piston core, Ca^{++} rose from 10 mmol kg^{-1} (the bottom water value) to >50 mmol kg^{-1} (a basement value) within 4 m of the seafloor [*Langseth et al.*, 1988].

Nonlinearity in these piston core gradients, consistently convex up, suggested that vertical pore water advection was largely responsible for the transport of ionic species in these sediments [*Langseth et al.*, 1988]. Vertical fluid flow velocities inferred from pore water gradients in piston cores and an analysis patterned after *Bredehoeft and Papadopulos* [1965] vary from <1 to 6 mm yr^{-1} [*Langseth et al.*, 1988]. With a fluid velocity of 1 mm yr^{-1}, it would take hundreds of thousands of years for pore water to move through several hundred meters of sediments, suggesting that the driving force for advection has existed for at least this long. In addition, there is also a positive correlation between geochemical gradients and measured heat flow [*Langseth et al.*, 1988] although fluid flowing upward through sediments at 6 mm yr^{-1} in a region with background heat flow of about 200 mW m^{-2} should have little influence on near-surface thermal gradients [*Langseth and Herman*, 1981; *Fisher*, 1989].

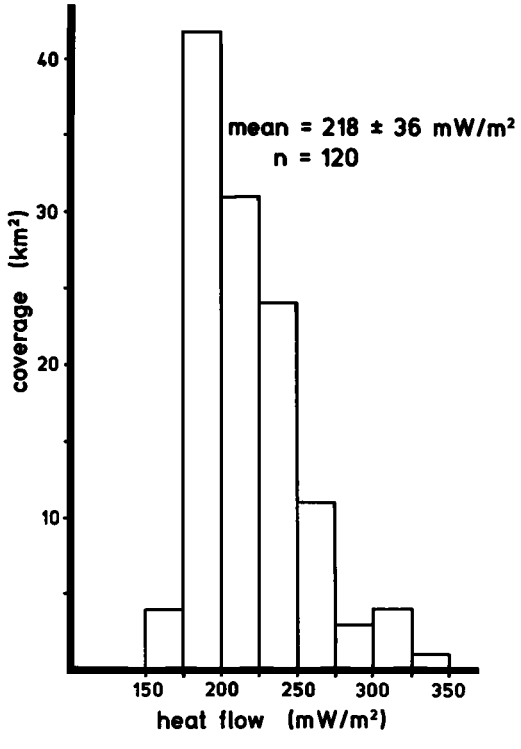

Fig. 5. Histogram, mean, and standard deviation of average heat flow values within 120, 1 by 1 km squares in the site 504 survey area. Scattered values were first evenly redistributed and smoothed [*Akima*, 1978]. The mean is slightly higher than that determined by *Langseth et al.* [1988] due to differences in the averaging schemes used in each analysis.

Profiles of Ca^{++} and Mg^{++} in pore fluids squeezed from sediments recovered at ODP Sites 677 and 678 also vary inversely, as in earlier piston cores. Concentrations of both elements were about the same at the seafloor and the sediment/basement interface beneath the two sites, despite large differences in heat flow and sediment thickness. The tendency of sediment pore fluids to approach the same composition near basement, as defined by 13 chemical species, suggests a large degree of homogeneity in basaltic pore fluids [*Mottl et al.*, 1983*b*, 1985; *Mottl*, 1989] and may be indicative of lateral pore fluid advection in the upper crust [*Langseth et al.*, 1988]. At low heat flow site 677, the profiles were convex down, while at high heat flow site 678, the profiles curved convex up, suggesting vertical fluid flow through the sediments at one to several millimeters per year [*Mottl*, 1989]. Fluid appears to be moving downward at low heat flow site 677 and upward at higher heat flow site 678. Thinner sediment cover over basement ridges may be localizing upward fluid flow and allowing lateral propagation of basement geochemical signals [*Mottl*, 1989].

A Summary of Observations and Inferences Concerning site 504

The geothermal and geochemical data collected near site 504 suggest the following:

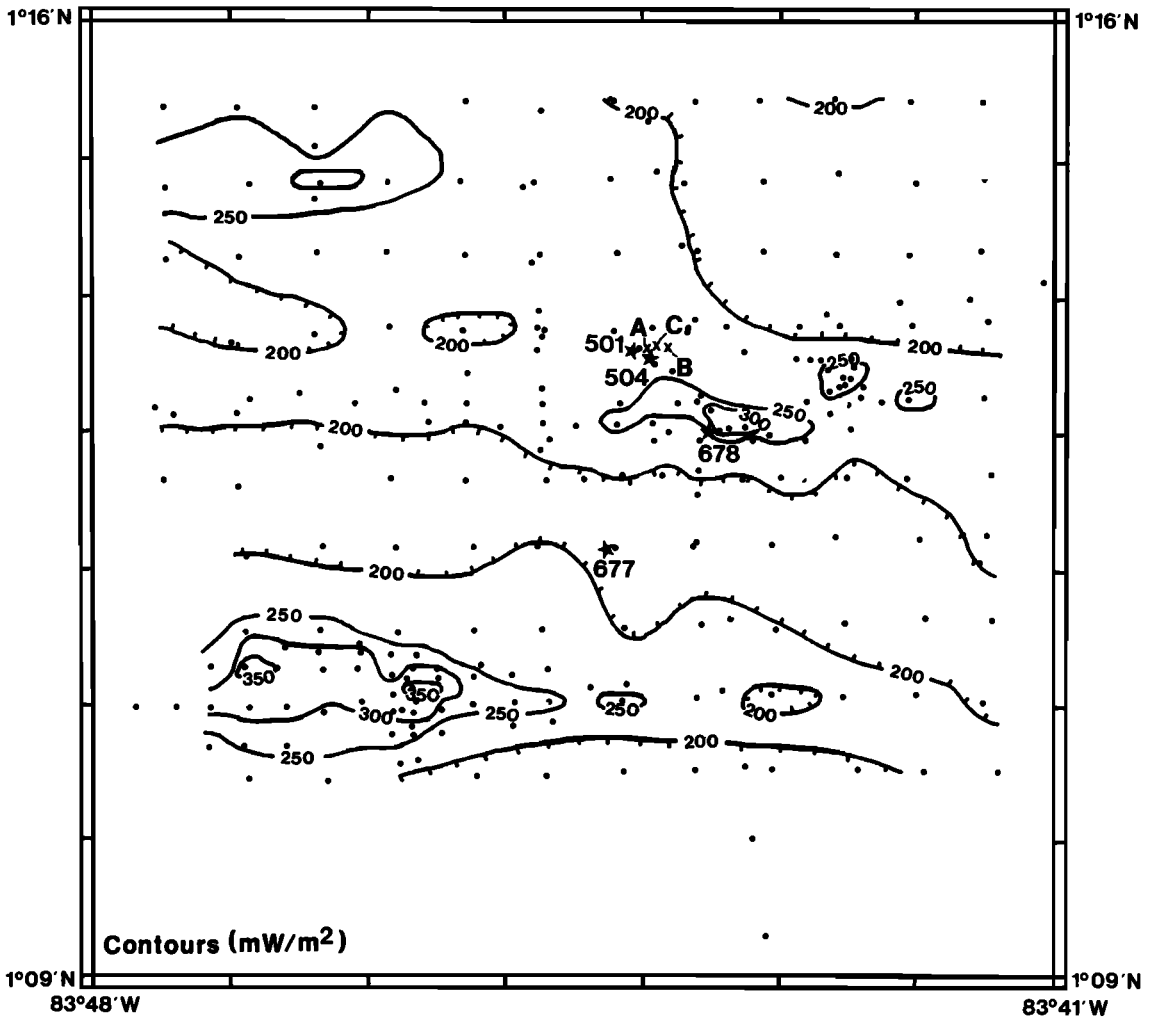

Fig. 6. Hand-contoured heat flow data from near site 504, collected during TT-198 and a 1982 *Robert D. Conrad* cruise [*Langseth and Mottl*, 1982; *Langseth et al.*, 1988]. The area of concentrated heat flow measurements is approximately 10 by 12 km.

1. There is a good correlation between heat flow, bathymetry, and geochemical gradients, as documented with data collected over a 10 by 12 km area. There is also an apparent correlation between these parameters and sediment thickness, although this relationship is suggested based on definite sediment thickness data from drilling at only three sites, separated by about 3 km.

2. Surface heat flow varies about a mean near that predicted for crust of 5.9 Ma age. This observation, together with a lack of significant curvature in shallow thermal gradients measured in 270 locations, suggests that conductive processes dominate heat transfer through the sediments near site 504.

3. Geochemical evidence from shallow piston cores, deep sediment cores, and basement sampling suggests that fluid is moving vertically and laterally through the sediments and upper crust. This inference does not conflict with observation 2 because the inferred flow velocities through sediments of several millimeters per year would not substantially influence the shallow thermal structure in the sediment column. Fluid appears to be moving upward over ridges (and local heat flow highs) and downward over troughs (and local heat flow lows).

4. An underpressure of about 8 bars has been documented in the upper 200 m of basement in hole 504B. This observation appears to require some form of crustal convection in order to maintain a dynamic condition.

There are several problems in reconciling these observations and suppositions with previous models of heat flow and crustal convection. Fluid flow at velocities of only millimeters per year should have little direct influence on regional heat flow. What then is the relationship between vertical and lateral fluid flow through the sediments, lateral fluid flow through the upper crust, and variations in surface heat flow of up to 100%? Can vigorous convection which is confined to basement be responsible for these observations? Numerical models of off-axis convection tend to result in convective cells extending a kilometer or more into the crust [*Green*, 1980; *Fehn and Cathles*, 1979, 1986; *Anderson and Zoback*, 1982; *Williams et al.*, 1986]. Can there be deep crustal convection in this area if the bulk permeability of basalt is $\leq 10^{-17}$ m^2 below the upper few hundred meters [*Anderson et al.*, 1985; *Becker*, 1989]? What is the relationship between convection confined to basement and fluid motion in the overlying sediments?

In earlier numerical models of off-axis convection, the sediment layer has either been ignored or assumed it to be impermeable. How important is the sediment layer in modifying passive convection? Can passive convection drive both vertical and lateral fluid flow through thick sediments? Given the moderate mean heat flow in this region and the apparently high hydraulic impedance of the sediments and most of the basalt, can passive convection in the upper crust dynamically maintain an underpressure of several

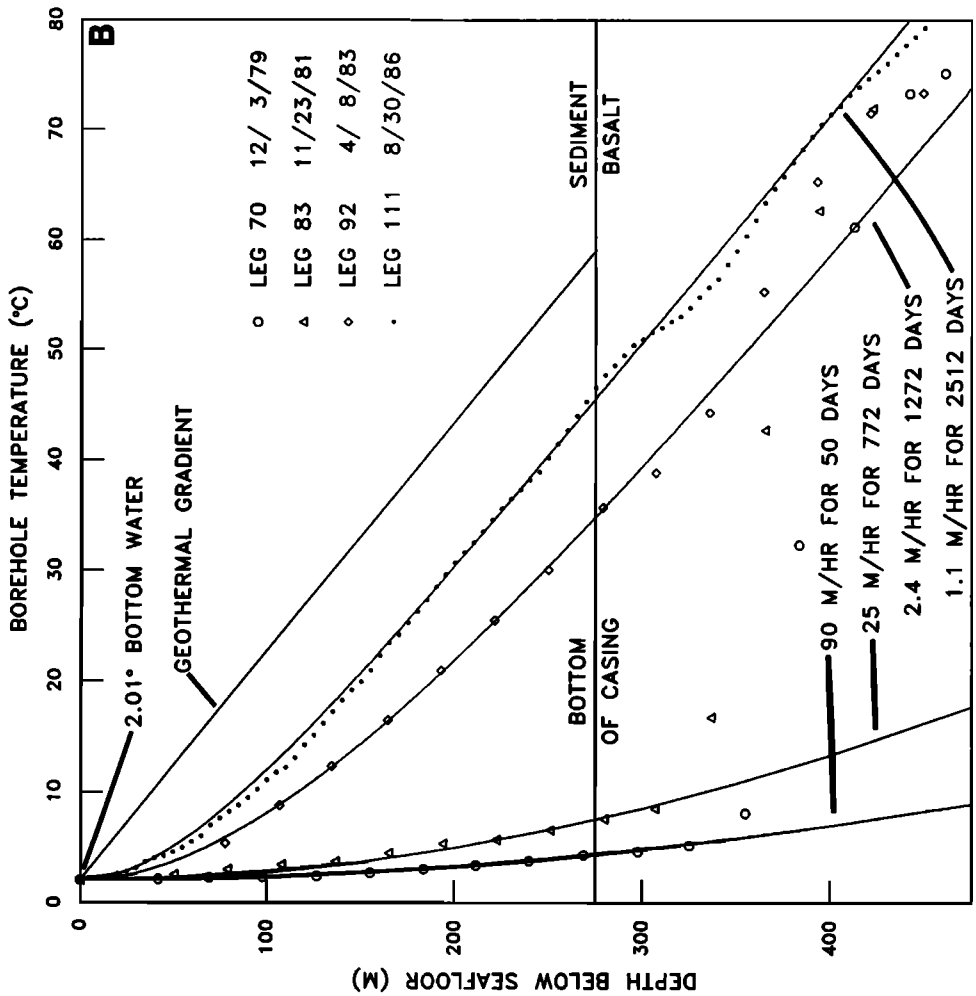

Fig. 7. (*a*) Temperatures measured in sediments in DSDP hole 504C during leg 69 and equilibrium open-hole temperatures measured in hole 504B during legs 69, 70, 83, 92 and 111 [*Becker et al.*, 1988]. (*b*) Equilibrium temperatures in the upper part of hole 504B and profiles predicted by the constant downhole flow rate model of *Becker et al.* [1983 *a*]. Note that the flow rate has decayed significantly over the 7 years since drilling on leg 69 penetrated the sediment seal above the upper crust.

bars in basement [e.g., *Williams et al.*, 1986]? Must site 504 be located over a downwelling or upwelling convection cell limb [e.g., *Anderson and Zoback*, 1982] or is the underpressure the same everywhere in basement?

In the next sections we have attempted to reconcile the various geological, geochemical, and geothermal observations near site 504. We present a brief analysis of heat flow, thermal conductivity, and sediment thickness which suggests that heat flow fluctuations in this area can be largely attributed to variations in thermal conductivity and sediment thickness, provided that temperatures in the upper basement have been kept relatively uniform by fluid circulation. We examine the role of convection through sediments and shallow and deep crust in creating underpressures and driving horizontal and vertical fluid flow and use analytical and numerical techniques to demonstrate that heat input from below the crust and topographic variations resulting from basement relief and uneven sediment drape may have combined to induce lateral pressure and temperature gradients, causing significant passive convection through sediments and the upper basement.

VARIATIONS IN CONDUCTIVE HEAT FLOW NEAR SITE 504

Langseth et al. [1988] and *Mottl* [1989] have suggested that partial chemical and thermal homogenization of basaltic pore fluids may have resulted from fluid flow at velocities of several to several tens of centimeters per year through upper basement near site 504. The thermal data have been inverted over two locations (besides DSDP site 504) where sediment thickness is known with certainty, ODP sites 677 and 678, to test this hypothesis.

Porosity (ϕ) and thermal conductivity (λ) data collected in sediment holes 504C, 677A, 677B, and 678B are compiled in Figure 8. Porosity decreases consistently with depth from about 85% at the surface to 65% at 250 m beneath the seafloor (mbsf). These porosities are somewhat higher than predicted by *Hamilton* [1976] for typical calcareous oozes, perhaps because of the relatively high sedimentation rate and variable concentrations of siliceous material. Sediment thermal conductivity data are more scattered, but values from all three sites follow similar trends. Conductivity is uniform or increases only slowly from the surface to about 130 mbsf, increases rapidly to about 160 mbsf, and then increases slowly again with depth. The break in slope occurs at approximately the same level as a shift in sediment composition, from dominantly carbonate material in the older sediments to mainly siliceous and pelagic sediments nearer to the surface [*CRRUST*, 1982]. Several geochemical gradients, most notably in Mg^{++} and Ca^{++} at site 677, also shift over this depth range, perhaps indicating the presence of a diagenetic boundary [*Mottl*, 1989].

Site 677 is located in a topographic trough, adjacent to a heat flow measurement of 166 mW m^{-2}. The linear thermal gradient indicated by a least squares best fit of the three sediment temperatures measured at this site on ODP leg 111, forced through a bottom water temperature of 2.01°C at mudline, is about .21°C m^{-1} to 93.1 mbsf [*Becker et al.*, 1988]. This gradient yields an estimated heat flow of about 177 mW m^{-2} [*Becker et al.*, 1988], and a temperature of 21.4°C at 93.1 mbsf. After assuming an intermediate background heat flow value of 175 mW m^{-2} and the thermal conductivity structure presented in Figure 8, sediment temperatures were conductively continued downward, yielding a value of 56.9°C at the basement surface, 309 mbsf (Table 1).

Estimating the basement temperature at site 678 was more difficult, since nearby heat flow measurements varied from about

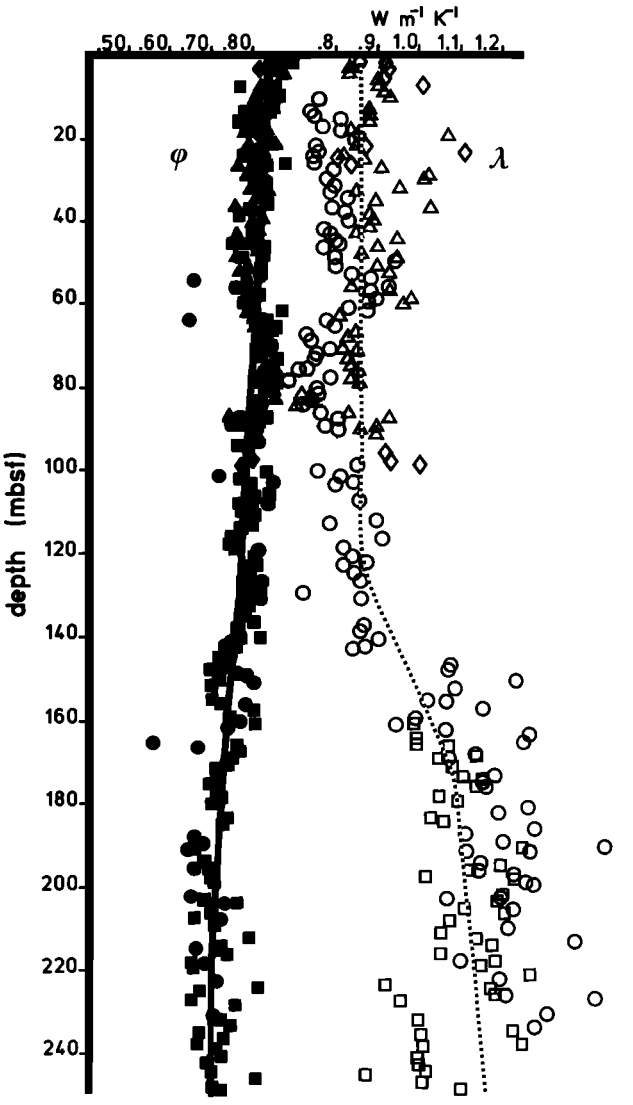

Fig. 8. Sediment porosity (ϕ) and thermal conductivity (λ) data from holes 504C (circles), 677A (squares), 677B (triangles) and 678B (diamonds) [*Wilkens and Langseth*, 1983; *Becker et al.*, 1988]. The curves were fit by eye.

250 to 325 mW m^{-2} over only a few hundred meters. After assuming an intermediate value of 290 mW m^{-2}, the same inversion procedure yielded a basement temperature of 58.2°C at 172 mbsf beneath site 678 (Table 1). The predicted basement temperatures of 56.9°C at site 677 and 58.2°C at site 678 are close to the sediment/basement interface temperature of about 58°C in hole 504C [*Becker et al.*, 1983*a*]. This analysis neglected the effect of vertical fluid movement at velocities of 1-2 mm yr^{-1} through the sediment column, as inferred from geochemical data at both sites [*Langseth et al.*, 1988; *Mottl*, 1989]. The estimated basement surface temperatures would be higher beneath sediments of the same thickness where fluid flow is directed downward and lower where flow is directed upward [i.e., *Sleep and Wolery*, 1978]. With a 170 m sediment layer at site 678, however, the temperature difference due to upward flow at 2 mm yr^{-1} would be only about 1°C. Similarly, a downward fluid flow velocity of 2 mm yr^{-1} at site 677 [Mottl, 1989] would result an estimated sediment/basement interface temperature only 2°C higher from

TABLE 1. Estimated Temperatures in the Sediment Column and at the Sediment/Basement Interface Beneath ODP Sites 677 and 678

Depth, mbsf	λ_e, W m^{-1} K^{-1}	T_{677}, °C	T_{678}, °C
0	-	2.0	2.0
0-5	0.75	-	3.9
5-10	0.83	-	5.7
10-30	0.85	-	12.5
30-120	0.86	26.8	42.9
120-130	0.89	28.8	46.1
130-140	0.94	30.7	49.2
140-150	0.98	32.5	52.2
150-160	1.03	34.2	53.9
160-170	1.07	35.8	55.0
170-180	1.08	37.4	57.7
180-190	1.09	39.0	-
190-200	1.11	40.6	-
200-210	1.12	42.2	-
210-220	1.13	43.7	-
220-230	1.14	45.2	-
230-240	1.15	46.8	-
240-250	1.16	48.3	-
250-260	1.17	49.8	-
260-270	1.18	51.3	-
270-280	1.19	52.7	-
280-290	1.20	54.2	-
290-300	1.21	55.6	-
>300	1.25	-	-
172	-	-	58.2
309	-	56.9	-

Temperatures were calculated after assuming purely conductive heat transfer through the sediments. Thermal conductivity data are from the dashed line from Figure 8. The sediment section was divided into 5- and 10-m thermal conductivity intervals. Where intervals are greater in thickness than 10 m (e.g., 30-120 mbsf), thermal conductivity was assumed to be constant over this depth range. The temperatures shown are those predicted at the base of each depth interval. At site 677, three temperature measurements were made in the sediments to a depth of 93.1 mbsf, so the first estimated temperature is for 120 mbsf. Heat flow at sites 677 and 678 was estimated to be 175 and 290 mW m^{-2}, respectively.

that determined conductively. Thus based on the data available from the three drill sites and the assumptions discussed previously, the temperatures at the top of basement may be fairly uniform in this area.

These results have been extended to the entire area near site 504 by assuming that (1) the thermal conductivity data combined from sites 504, 677 and 678 (Figure 8) are representative of the 120 km^2 field area; (2) the sediment/basement interface has a temperature near 58°C everywhere within this area; (3) surface heat flow variations can be entirely attributed to differences in sediment thickness with fixed upper and lower boundary temperatures; and (4) vertical conduction of heat through the sediments is significantly more important than either lateral conduction or fluid advection of heat. The heat flow data set of 242 values was then inverted to yield estimated sediment thicknesses at each station; these scattered data were machine contoured with an interpolation scheme [*Akima*, 1978] to yield a synthetic isopach map of the survey area (Figure 9).

This analysis produced an end-member case; the resulting isopach map is likely to be somewhat more extreme in identifying lateral variations in sediment thickness than exist in the natural system, since deviation from assumptions 2 to 4 above will tend to reduce the conductive effects of differential sediment thickness. This propensity was somewhat offset, however, by machine regridding and the contouring of unevenly distributed estimates of sediment thicknesses at a large interval. This exercise was intended primarily to determine the range of variations in sediment thicknesses expected in the survey area; an error in the predicted basement temperature of 5°C will result in a sediment thickness error of about 30 m. The inversion of thermal data to derive sediment thicknesses is certainly less accurate than a careful analysis of good seismic data.

Water depth data from the 242 stations used to produce the heat flow map in Figure 9*a* were also machine-contoured to generate a map of bathymetry near site 504 (Figure 10*a*). We used a more limited raw data set than that of *Langseth et al.* [1988] so that the synthetic isopach and bathymetric data (Figures 9*b* and 10*a*), could be combined to produce a synthetic basement topography map (Figure 10*b*). This basement surface map suggests that the amplitude of basement relief is about 200 m in the site 504 field area. These predicted variations in sediment thickness and in basement elevation are used in later numerical models of passive circulation through the oceanic sediments and crust.

PASSIVE CONVECTION NEAR SITE 504

Hydraulic Impedance and Unevenly Draped Sediment

Karato and Becker [1983] defined the hydraulic impedance of a sediment layer of thickness h to be

$$I(h) = \int_0^h \frac{dz}{k[\phi(z)]} \tag{1}$$

where ϕ is porosity and k is absolute permeability. The compiled sediment porosity data from near site 504 (Figure 8) fall between the deep sea "pelagic" and "carbonate ooze" curves from *Hamilton* [1976], and yield a best fit, second-order polynomial of

$$\phi = 0.857 - 0.415z - 2.010z^2 \tag{2}$$

where z is depth in kilometers.

We have assumed that the *Bryant et al.* [1974] porosity/permeability relationship for deep sea sediments applies near site 504, allowing permeability to be calculated directly from void ratio ($e = \phi / [1 - \phi]$):

$$k = 10^{-18} e^5 \tag{3}$$

The resulting permeability values are about the same as those measured by *Morin and Silva* [1984] on a calcareous ooze, collected by piston core from the GSC, over the 75-85% porosity range, where the two analyses overlap. When equations (2) and (3) are substituted into equation (1), the relationship between sediment impedance and depth reduces to

$$I(h) = 10^{18} \int_0^h \left[\frac{0.071 + 0.207z + z^2}{0.426 - 0.207z - z^2}\right]^5 dz \tag{4}$$

Equation (4) was integrated numerically (Carnahan et al., 1969) for a range of sediment thicknesses (Figure 11). Interestingly, the impedance of a 150-m sediment column is one order of magnitude less than that of a 250-m sediment column, even though the difference in sediment thickness is only 40%. This difference in

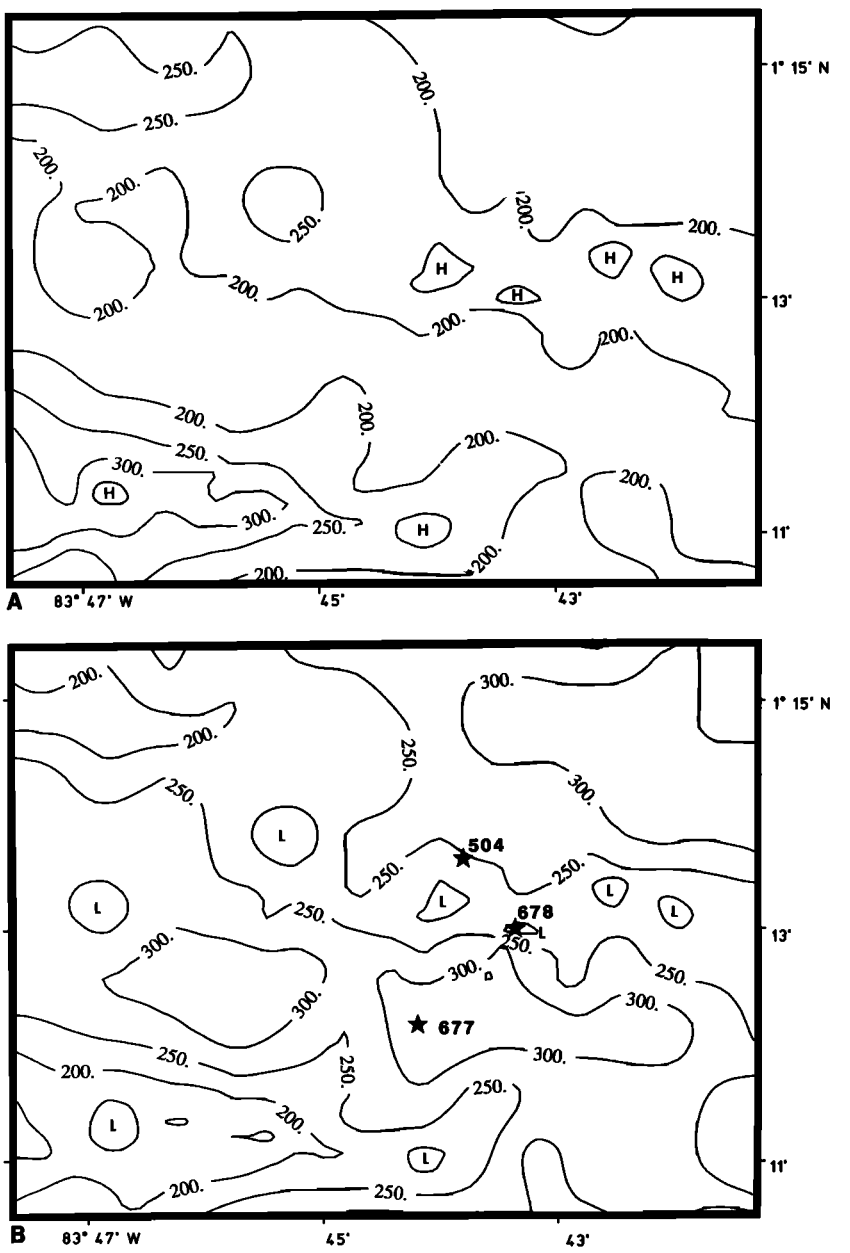

Fig. 9. (*a*) Machine-contoured heat flow data from a 10 by 12 km area near site 504. Data include 242 scattered values from near site 504 which were evenly redistributed with a linear interpolation scheme [*Akima*, 1978]. (*b*) Synthetic isopac for the area near site 504 created by inverting heat flow data from Figure 9a, assuming isothermal surfaces above (2°C) and below (58°C) the sediment layer, surface thermal conductivity of 0.75 W m^{-1} K^{-1}, and a thermal conductivity/depth relationship shown with the dotted line in Figure 8. This analysis was also based on the assumption that heat transfer through the sediment column is dominantly conductive. A difference of 5°C at the sediment-basement interface would result in a change in calculated sediment thickness of about 30 m.

sediment impedance, when superimposed on basement relief, may modify fluid circulation in the upper oceanic crust near site 504, as will be demonstrated with numerical methods.

Subcritical Convection in the Natural System

The expected Rayleigh number R_a for a saturated, porous medium may be calculated as:

$$R_a = \frac{\alpha g k H \Delta T}{\upsilon \kappa_m} \quad (5)$$

where α is the coefficient of thermal expansion of the fluid, g is gravitational acceleration, k is matrix permeability, H is the thickness of the permeable layer, ΔT is the temperature difference across this layer, υ is kinematic viscosity, and κ_m is the thermal diffusivity of the fluid-saturated matrix. For an isotropic, homogeneous porous medium with impermeable, isothermal upper and lower surfaces, the critical value required to initiate free convection (R_c) is $4\pi^2$ (≈ 40) (Table 2) [*Lapwood*, 1948; *Nield*, 1968]. Assuming appropriate values for equation (5), including crustal permeability of 10^{-17} m^2 below the upper 200 m of basalt at site 504 [*Anderson et al.*, 1985; *Becker* , 1989], the Rayleigh number for this section of the oceanic crust is probably no higher that about 12. The estimated Rayleigh number in the upper 100 m of basalt, where permeability is about 10^{-13} m^2 is less than 9.

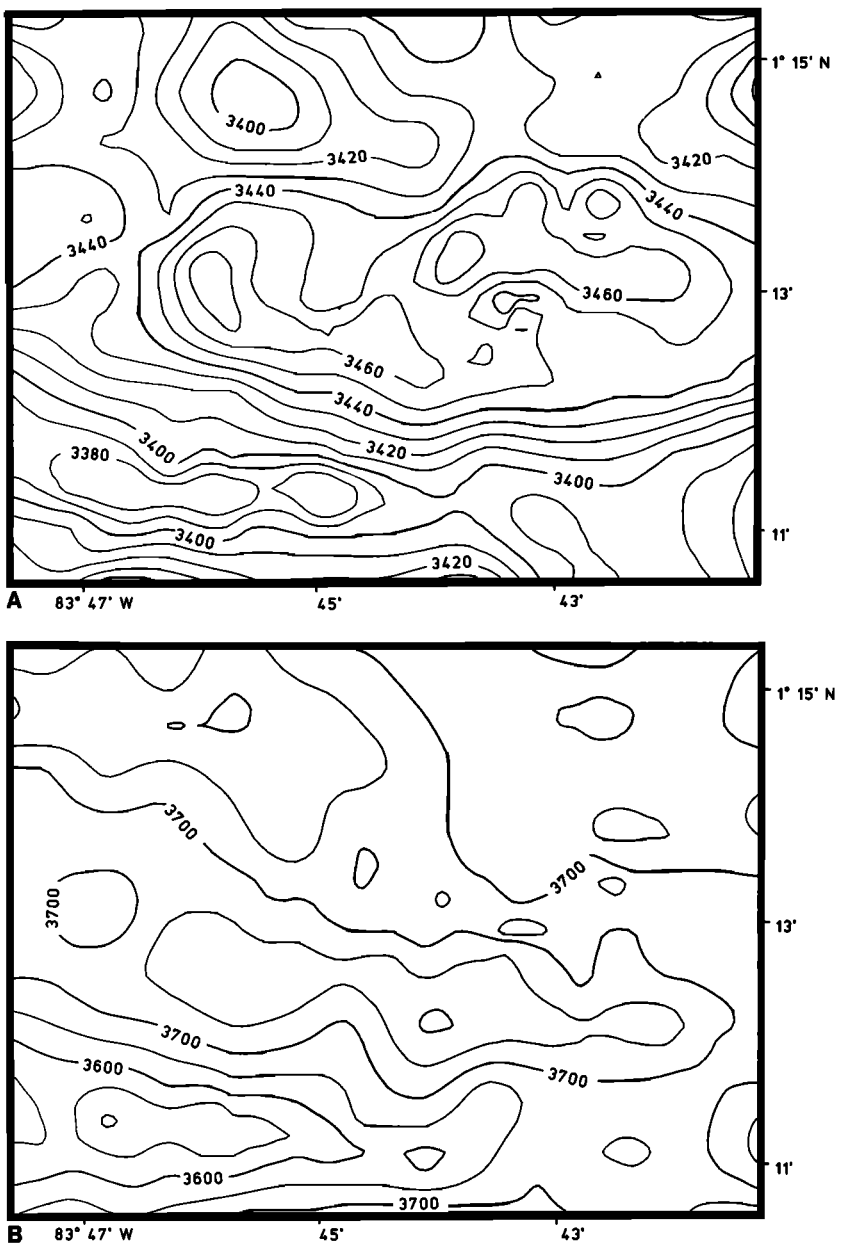

Fig. 10. (*a*) Machine contoured bathymetry, based on depths from the same 242 stations used to produce Figure 9 *a*. (*b*) Synthetic depth to basement map of the area near site 504 created by combining bathymetry (Figure 10*a*) with the synthetic isopach data (Figure 9*b*).

Thus passive convection in the crust beneath site 504 is certainly subcritical.

The tendancy for convection cells to form with particular aspect ratios only applies to critical and super-critical flow [*Lapwood*, 1948; *Nield*, 196]. Because free convection is probably sub-critical near site 504, it may not be reasonable to infer the depth of circulation from the length scale of surface heat flow anomalies, even if these data reflect the horizontal scale of convection. In addition, there is no evidence to suggest that circulation cells of any particular geometry are favored during any convection through heterogeneous, and possibly anisotropic, porous media. Although there is good evidence for fluid flow to depths of several kilometers at ridge crests [*Lister*, 1972, 1974; *Spooner and Bray*, 1977; *Gregory and Taylor*, 1981; *Campbell et al.*, 1988; *Vanko*, 1988] deep convection may not be possible on ridge flanks. In the following analyses, it is demonstrated that shallow convection through only the upper crust is consistent both with this interpretation of Rayleigh numbers in the natural system and many observations near site 504.

Topographically Forced Convection

Lister [1972] suggested that topographically forced convection could be responsible for a correlation between heat flow and bathymetry on the heavily sedimented flank of the Juan de Fuca Ridge, with higher values measured over ridges and lower values in troughs. *Lowell* [1980] and *Hartline and Lister* [1981] argued that topography induced horizontal temperature gradients which could drive sub-critical convection ($R_a < R_c$), in which the cell size was determined by topographic wavelength.

Lowell [1980] analyzed the influence of topographic forcing on subcritical hydrothermal convection in oceanic crust, by casting

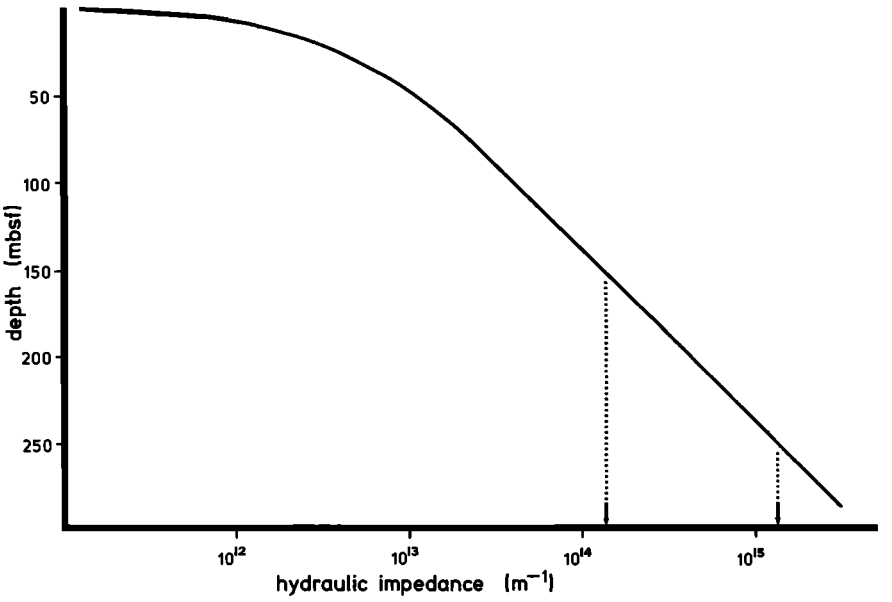

Fig. 11. Hydraulic impedance of the sediments near site 504, determined with equation (5) over a range of depth intervals. The arrows indicate impedance values determined for 150 and 250 m of sediment.

TABLE 2. Calculated Critical Rayleigh Number R_c, Wave Number ξ and Convection Aspect Ratio ζ for Circulation in a Homogeneous, Porous Medium with Varying Boundary Conditions

Boundary Conditions				R_c	ξ	ζ
Fluid Flow Conditions		Thermal Conditions				
Bottom	Top	Bottom	Top			
I	I	T_b	T_t	$4\pi^2$	π	2.00
I	I	T_b	Q_t	27.10	2.33	2.70
I	I	Q_b	Q_t	12.00	0.00	∞
I	P	T_b	T_t	27.10	2.33	2.70
$\Rightarrow$ I	P	Q_b	T_t	17.65	1.75	3.59
$\Rightarrow$ I	P	T_b	Q_t	9.87	1.57	4.00
I	P	Q_b	Q_t	3.00	0.00	∞
P	P	all	all	0.00	0.00	∞

Fluid flow conditions are either permeable (P) or impermeable (I). Thermal conditions may be fixed temperature T or fixed heat flux Q, with subscripts indicating top t or bottom b boundaries. The arrows indicate conditions which seem the most likely for the natural Costa Rica Rift, off-axis hydrothermal system. Table modified from *Nield* [1968] after *Green* [1980].

the problem in terms of coupled heat and fluid flow through both unsedimented and sedimented basalt. In an analysis of unsedimented oceanic crust, *Lowell* [1980] constructed an idealized two-dimensional cross section through the crust, oriented parallel to the major plane of convective motion, and found a first-order solution to the critical equations for vertical fluid flow:

$$w_1(x,0) = \frac{\alpha g \gamma k d}{4 \nu} \cos \xi x \left[1 - 2\xi H \operatorname{csch}(2\xi H)\right] \qquad (6)$$

where w_1 is the first order vertical fluid velocity, γ is the thermal gradient, ξ is topographic wave number, H is the thickness of the permeable (hydrothermal) layer, and the other variables are defined as before. Topography was approximated by the inclusion of boundary conditions which established lateral temperature gradients at the upper boundary of the domain but neglected lateral pressure gradients.

Assuming reasonable values of $\alpha = 5.32 \times 10^{-4}$ K^{-1}, γ = 0.10°C m^{-1}, $\upsilon = 4.44 \times 10^{-6}$ m^2 s^{-1}, and a deep crustal permeability k_b of 10^{-17} m^2, we have calculated vertical fluid velocities through the oceanic crust in four extreme cases, with circulation reaching depths of 1500-5000 m and basement topographic variations of 200-300 m (Table 3). The highest predicted fluid velocities are 0.017-0.027 mm yr^{-1}, 3 orders of magnitude smaller than those suggested by geochemical analyses of pore waters from sediment cores [*Langseth et al.*, 1988; *Mottl*, 1989]. Because the thick sediment blanket which covers the crust at site 504 has been ignored, the calculated velocities will be an upper limit. It is clear that the present scale of basement relief has little influence on fluid circulation in the deep crust near site 504.

It is possible that convection is confined to the upper several hundred meters of permeable crust beneath site 504. Assuming a maximum depth of circulation of 300 m into the shallow basalt,

TABLE 3. Maximum Fluid Velocities Predicted Using the Analysis of *Lowell* [1980] for Subcritical Convection Forced by Topography

Amplitude of topographic variation, m	Thickness of hydrothermal layer, m	
	1500	5000
200	0.017	0.018
300	0.025	0.027

The hydrothermal layer is assumed to be entirely basalt, open to free communication with the overlying ocean. Crustal permeability was assumed to be 10^{-17} m^2 [*Anderson et al.*, 1985], and velocities are in mm yr^{-1}.

bathymetric relief of 200 m and a bulk basalt permeability of 5×10^{-15} m^2 (probably an over estimate for the upper 300 m), the calculated maximum vertical fluid velocity is 1.24 mm yr^{-1}. In the natural system, the "permeable" section of basalt is ≤200 m in thickness (and the most permeable section may be less than 100 m in thickness) [*Anderson and Zoback*, 1982; *Anderson et al.*, 1985; *Becker*, 1989], but the *Lowell* [1980] analysis breaks down unless the thickness of the convecting layer is less than the height of the topographic variation.

Lowell [1980] also analyzed the effects of sediment cover over wave like crustal topography, but assumed that the upper sediment surface was flat, making the upper boundary both isothermal and isobaric. In addition, solutions were determined only for cases where $\xi H \gg 1$, a condition not satisfied near site 504 where $\xi H \approx 0.16$. Fluid velocities were reduced in comparison to the sediment-free case, due to the presence of the uneven sediment blanket, and *Lowell* [1980] concluded that topographically forced convection might be important in moderately to thickly sedimented crust, provided that the permeability contrast at the sediment/basalt interface was not too large.

This nonnumerical approach is limiting because it does not allow inclusion of realistic heterogeneities, physical properties, or boundary conditions. Topographic relief may create shallow, horizontal pressure gradients sufficient to drive subcritical fluid circulation [*Hartline and Lister*, 1981], but it has thus far not been possible to quantify fluid flow rates or pressure differences in the natural system. In the next sections, we have used numerical techniques to elucidate the characteristics of an off-axis, passive convection system in the southern flank of the CRR.

NUMERICAL MODELS OF PASSIVE CONVECTION

Governing Equations of the Mathematical Model

The mathematical model simulates fluid and heat transport in a porous medium by balancing mass and energy. These two quantities are conserved through equations expressed in integral form:

$$\frac{\partial}{\partial t}\int_V \phi \rho \, dV = -\int_V \rho \, \mathbf{v}_d \cdot \mathbf{n} \, dA + \int_V G_f \, dV \qquad (7)$$

$$\frac{\partial}{\partial t}\int_V \rho \, e_f \, dV = -\int_A c_f \delta T \, \mathbf{v}_d \cdot \mathbf{n} \, dA + \int_A \lambda \nabla T \cdot \mathbf{n} \, dA + \int_V G_n \, dV \qquad (8)$$

where ϕ is medium porosity, ρ is fluid density, $\mathbf{v}_d$ is Darcy velocity, $\mathbf{n}$ is a unit vector normal to surface area A, V is volume, c_f is fluid specific heat, ΔT is the temperature at surface segment dA, λ is thermal conductivity, e_f is the fluid internal energy, and G_f and G_n are fluid and energy production terms (these last two terms were not used in the following analysis).

These two equations are coupled through the pressure and temperature fluid-property dependency, and through the convection terms (the first terms on the right-hand side of both equations (7) and (8)) which transport fluid and heat. Fluid flow velocities were calculated assuming Darcy's law (in vector form):

$$\mathbf{v}_d = -\frac{k}{\mu}(\nabla P - \rho g) \qquad (9)$$

for porous media where k is absolute permeability, μ is fluid viscosity, P is fluid pressure and g is gravitational acceleration. Fluid density, expansivity, compressibility, and specific heat are all treated as functions of pressure and temperature according to an equation of state for pure water [*Haar et al.* 1984], which has been calibrated from $260 \le T \le 2500$ K and $0 \le P \le 3000$ MPa (30,000 bar) with an estimated accuracy better than 3.5 ppt for density and specific enthalpy [*Haar et al.*, 1984]. We adapted this equation of state to calculate water properties at each time step in our simulations and verified our formulation by comparing calculated properties to those listed in steam tables [*Keenan* et al., 1969; *Haar et al.*, 1984]. Fluid viscosity was calculated using the formulation of *Kestin* [1978].

The left-hand side of (7) includes compressibility and expansivity terms:

$$\frac{\partial}{\partial t}\int_V \phi \rho \, dV = V \phi \rho \left[\beta_t \frac{\partial P}{\partial t} - \alpha_t \frac{\partial T}{\partial t}\right] \qquad (10)$$

where β_t is the total compressibility of the water-rock system and α_t is total expansivity.

Equations (7)-(9) are thus nonlinear with both pressure and temperature dependence as defined by the equation of state and equation (10), and are fully coupled in a program called PT [*Bodvarsson*, 1982]. This code is based on the integrated finite difference method [*Narasimhan and Witherspoon*, 1976] and is designed to handle multidimensional, anisotropic, heterogeneous systems. Originally developed for geothermal reservoir analysis, PT can handle free and forced convection and has been extensively analyzed and verified [*Bodvarrson*, 1982; *Javandel et al.*, 1984; *Tsang and Doughty*, 1985; *Mangold and Tsang*, 1987].

Two-dimensional Models of Passive Convection

An examination of bathymetry and heat flow near site 504 (Figures 2 and 6) reveals strong east to west trends. We have assumed that the fluid convection pattern through the ocean crust can be idealized with primary orientation north to south, perpendicular to structural strike [*Straus*, 1974; *Fehn and Cathles*, 1979, 1986; *Fehn et al.*, 1983; *Morton and Sleep*, 1985; *Langseth et al.*, 1988], which allowed the use of a finely gridded, two-dimensional modeling mesh. Downhole experiments and logging have continued in hole 504B to a depth of 1535 mbsf [*Becker et al.*, 1989], setting a minimum depth for these simulations. While the permeability structure below this depth in the oceanic crust is unknown, a modeling domain 5 km deep was chosen for the first set of simulations to test the possibility of whole crustal convection. The modeled section varied from 10 to 20 km in width and was intended to represent a cross section

through the seafloor across site 504. The simulations were run with a range of porosity and permeability values; standard depth/porosity and porosity/permeability curves for deep sea sediments [*Bryant et al.*, 1974; *Hamilton*, 1976; *Morin and Silva*, 1984] and data from DSDP legs 69, 70, 83, and 92 and ODP leg 111 [*CRRUST*, 1982; *Cann et al.*, 1983; *Anderson et al.*, 1985; *Becker et al.*, 1988, 1989] provided the baseline physical properties values.

The simulations were split into three stages, each designed to test specific aspects of the hydrogeological regime (Table 4). The first two stages included planar simulations, with a flat upper boundary and horizontally distributed, layered heterogeneities, as have been commonly assumed with hydrogeological models of the oceanic crust (Figure 12) [e.g., *Fehn and Cathles*, 1979; *Green*, 1980; *Fehn et al.*, 1983; *Williams et al.*, 1986]. The third series of simulations included more realistic geometry, designed to

TABLE 4. Summary of Model Dimensions and Characteristics.

	Planar Simulations		Topographic Simulations
	Stage 1	Stage 2	Stage 3
Section length, km	10-20	10	10
Section height, km	5.0	1.5	1.0
Horizontal divisions	25	25	25
Element length, m	400-800	400	400
Vertical divisions	15	30	28-32
Element height, m	50-500	25-100	25-100
Total elements	375	750	750
Sediment types	3	10	10
Sediment thickness, m	250	250	150-250
Basalt types	6	5	4
Basalt thickness, km	4.75	1.25	0.75
Variable bathymetry	no	no	yes
Sediment drape	no	no	yes

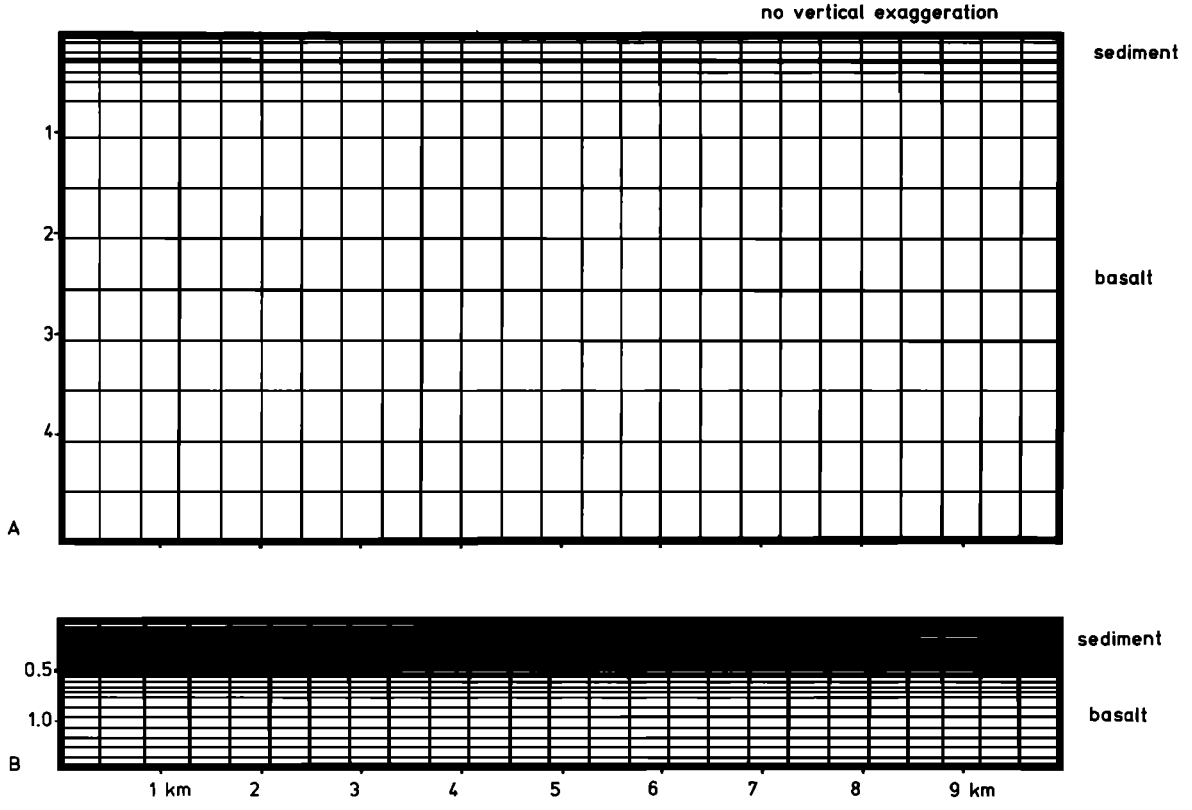

Fig. 12. Two meshes used in studies of a planar cross section through oceanic sediments and crust on a ridge flank. Material types and physical properties are summarized in Table 5; parametric variations are listed in Table 6. Nodal dimensions were varied by a factor ≤2 from one element to the next. (*a*) stage 1 simulations: 250 m of sediment overlying 4750 m of oceanic crust; 375 total node-centered elements form 25 horizontal and 15 vertical divisions, representing a sediment and crust section measuring 10 by 5 km. This mesh includes three sediment and six basalt types. (*b*) stage 2 simulations: 750 total elements forming 25 horizontal and 30 vertical divisions, covering a sediment and crust section measuring 10 by 1.5 km. These simulations included the sediments and the upper portion of crust from stage 1 tests, with 10 sediment and three basalt types.

include the effects of variable basement topography, unevenly draped sediment, and subdued bathymetry (Figure 13). These last simulations included nonhorizontal, nonparallel layered heterogeneities in a 10 by 1 km domain.

Sediment and rock porosities, permeabilities, and thermal conductivities were input for 16 total material types, with porosities varying from 85 to 1% and permeabilities from 10^{-13} to10^{-25} m^2 in the standard cases (Table 5). Higher permeabilities were tested in additional simulations. All simulations were run to steady state after an arbitrary run time of 5×10^6 years. Steady state was assumed to have been achieved when over a time step $\Delta t \geq 2 \times 10^5$ yr the maximum $\Delta T \leq 0.001$°C and maximum $\Delta P \leq 0.0001$ bar for all nodes within the fluid flow domain. Model time steps varied from 10^{-6} to 6.3115×10^{12} s (2.0×10^5 years) over the length of the simulations; time steps were doubled when possible but halved whenever ΔT or ΔP exceeded maximum values of 5°C and 1.0 bar, respectively, in any node. Because sediment thickness, boundary conditions, and physical properties remained constant throughout the simulations, only steady state results were of interest; there was no attempt to include transient effects in these simulations.

Initial and Boundary Conditions and Parametric Variations

As all simulations were run until temperatures and pressures within all cells attained equilibrium, the choice of initial conditions was not critical. A purely conductive simulation was run to determine background thermal gradients and initial temperatures for each node. These background temperatures were then used to calculate fluid density and derive a "hot hydrostatic" pressure gradient, in which changes in the density of overlying fluid result from conductive heating from the surrounding matrix. A "cold hydrostatic" pressure gradient is one in which the fluid density shifts as a function of pressure only (a very small change as water is relatively incompressible) while the temperature of all fluid is fixed equal to that of bottom water (2.01°C). Conductive temperatures and hot hydrostatic pressures were used as initial conditions in all simulations, but cold hydrostatic pressures were used for comparison in later computations.

The top boundary was fixed at constant temperature (2.01°C) and made permeable. In planar simulations, the pressure at the top boundary was fixed at 346.6 bars, appropriate for a water depth of 3450 m. In topographic simulations, the pressure at the top boundary was assumed to be hydrostatic, but varied from 346.6 to 356.8 bars with a 100 m of relief.

At the lower boundary, a variable heat flow condition was assumed more realistic than either constant temperature or constant heat flow conditions used in many earlier models of hydrothermal circulation in young oceanic crust. Heat input varied as a function of crustal age according to the relation of *Parsons and Sclater* [1977], assuming that the field area has a mean age of 5.9 Ma and that the cross section is oriented perpendicular to a ridge axis with a half-spreading rate of 34 mm yr^{-1}. Unlike many other models [*Fehn and Cathles*, 1979, 1986; *Green*, 1980; *Fehn et al.*, 1983], it was not necessary to simulate heat input from the ridge crest in these experiments. Site 504 is located over 200 km

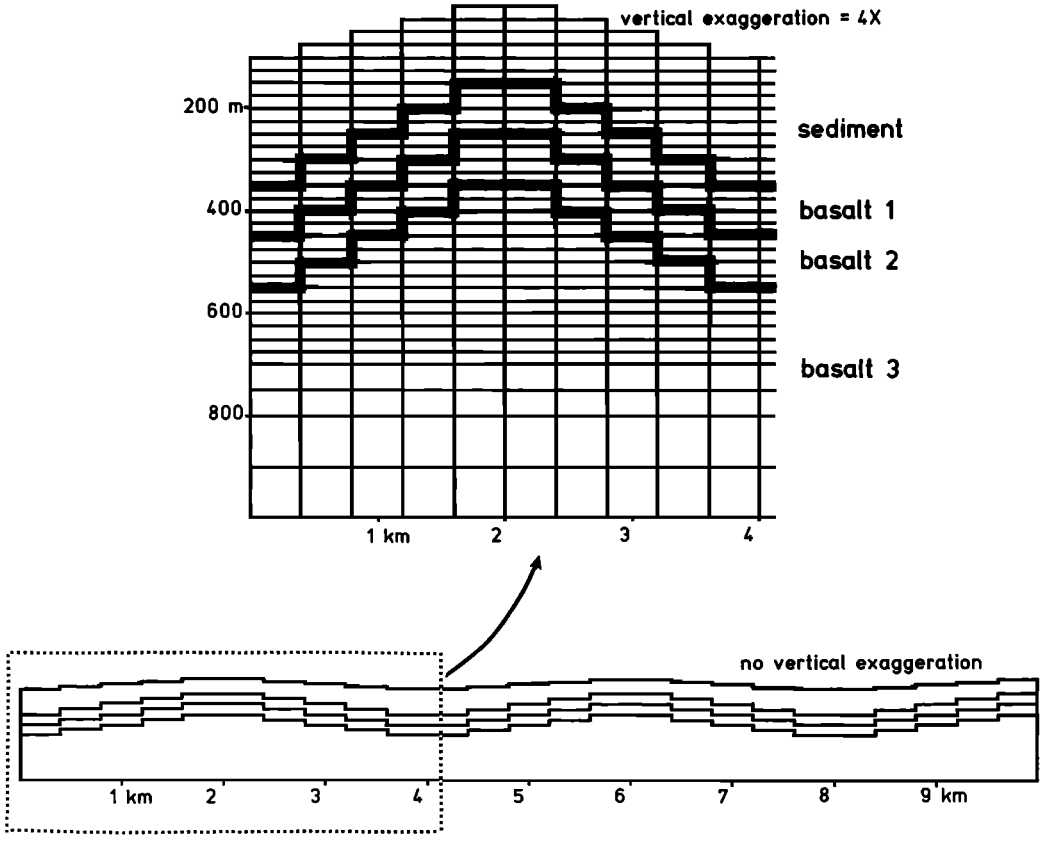

Fig. 13. Model mesh used to test the influence of basement relief and an uneven sediment layer on passive convection. Basement relief has an amplitude of 200 m and a wavelength of 4 km. Sediment thickness varies from 250 m over basement troughs to 150 m over basement ridges, and results in subdued bathymetric relief of just 100 m. This mesh contains 750 node-centered elements split by 25 horizontal and 28-32 vertical divisions. The sediment and basalt types and properties are summarized in Table 5.

TABLE 5: Summary of Sediment and Basalt Physical Properties Used in Numerical Simulations.

Depth, mbsf	Type	ϕ	e	λ, W m^{-1} K^{-1}	k, m^2
		Stage 1			
0-50	s	0.85	5.47	0.86	4.88×10^{-15}
50-150	s	0.80	3.89	0.89	8.88×10^{-16}
150-250	s	0.69	2.23	1.11	5.94×10^{-17}
		Stages 1 and 2			
0-25	s	0.85	5.73	0.85	6.20×10^{-15}
25-50	s	0.84	5.20	0.86	3.79×10^{-15}
50-75	s	0.82	4.66	0.86	2.19×10^{-15}
75-100	s	0.81	4.14	0.86	1.21×10^{-15}
100-125	s	0.78	3.65	0.87	6.46×10^{-16}
125-150	s	0.76	3.20	0.88	3.37×10^{-16}
150-175	s	0.74	2.80	1.03	1.71×10^{-16}
175-200	s	0.71	2.43	1.10	8.49×10^{-17}
200-225	s	0.68	2.11	1.12	4.14×10^{-17}
225-250	s	0.65	1.82	1.15	1.98×10^{-17}
		All Stages			
250-350	b_1	0.125	-	1.50	1.00×10^{-13}
350-450	b_2	0.10	-	1.60	5.00×10^{-15}
450-750	b_3	0.08	-	1.75	1.00×10^{-17}
750-950	b_3	0.05	-	1.85	1.00×10^{-17}
950-1500	b_3	0.01	-	2.00	1.00×10^{-17}
>1500	$b_{3,4}$	0.01	-	2.00	10^{-17} or 10^{-25}

Porosity ϕ and thermal conductivity λ values are from best fitting curves in Figure 8. Sediment permeabilities are from *Bryant et al.* [1974] and vary as a function of void ratio e. The different basalt types (b_1, b_2, b_3, and b_4) distinguish materials with different permeabilities. Note that b_3 includes basalt with three different porosity and thermal conductivity values, although permeability is always 10^{-17} m^2. For topographic tests, actual depths of individual basalt layers vary by up to 100 m although the thickness of each layer remains constant.

south of the CRR, too far from the axis for lateral transport of heat from the ridge to be important. The vertical boundaries were assumed impermeable and adiabatic, as in most numerical simulations of hydrothermal circulation in the oceanic crust [*Fehn and Cathles*, 1979, 1986; *Green*, 1980; *Fehn et al.*, 1983; *Williams et al.*, 1986], although this condition was tested. We were particularly concerned about using impermeable boundaries because we hoped to determine if there was a favored convection cell geometry which varied as a function of the depth of fluid penetration. In one parametric variation, the vertical sides of the simulated crustal section were held at constant hot hydrostatic pressure and temperature gradients. In another simulation, the domain width was doubled. The results of these two simulations demonstrated that the use of impermeable boundaries did not strongly influence the conclusions of this study.

Our model assumed that fractures or joints through which fluids circulate were close enough together to allow the use of Darcy's law and to allow full thermal equilibration between fluid and matrix. The thermal effects of sedimentation during modeling runs were ignored but are probably not critical with steady state input of about 50 mm kyr^{-1}. Planar simulations included 250 m of sediment overlying a basaltic crustal section with a total thickness of 1.5-5.0 km (Figure 12). As not much is known about lateral variations in sediment properties within the site 504 survey area, characteristics were assumed to vary most strongly with depth. Topographic simulations were the exception to this rule, as variable basement topography and sediment thickness created strong lateral as well as vertical gradients in properties. Sediment porosities and thermal conductivities from holes 504C, 677A, 677B and 678A provided the appropriate depth relations (equation (2) and Figure 8). Sediment grain density was found to be nearly constant throughout the column, 2650 ± 370 (s.d.) kg m^{-3} (421 samples) [*Wilkens and Langseth*, 1983; *Becker et al.*, 1988].

Sediment permeabilities k_s in all standard case simulations were determined from equations (2) and (3). As the exact porosity/permeability relationship in deep-sea sediments is not well understood, sediment permeability values 10 and 100 times higher than those determined with the *Bryant et al.* [1974] curve were also tested. Basalt porosities and permeabilities were determined from results of large-scale electrical resistivity [*Becker*, 1985] and packer experiments [*Anderson and Zoback*, 1982; *Anderson et al.*, 1985; *Becker*, 1989] (Figure 14 and Table 5). One crucial assignment was that of permeability in the upper 200 m of basalt. This section was divided into two, 100 m-thick sections with permeabilities of 10^{-13} m^2 and 5×10^{-15} m^2 in the standard simulations. The remaining basalt (everything below the upper 200 m of basement) was assigned a permeability $\leq 10^{-17}$ m^2 (Table 5) [*Anderson et al.*, 1985; *Becker*, 1988; *Becker et al.*, 1989]. These values are in strong contrast to those assigned in many earlier models of the oceanic crust when permeabilities many orders of magnitude higher than those in the natural system were tested.

In our standard case simulations, crustal basalt was made effectively impermeable, with $k_b = 10^{-25}$ m^2, for $z > 1500$ mbsf. In fact, the bulk permeability of crustal basalt below 1500 mbsf is unknown, but the purely conductive extreme chosen for the standard case is one reasonable end-member. The other extreme case, with permeable basalt below 1500 m, was tested as well. Figure 15 illustrates the layered permeability structure used in the standard case simulations. Permeability steadily decreases through the sediment column, increases by nearly 4 orders of magnitude in

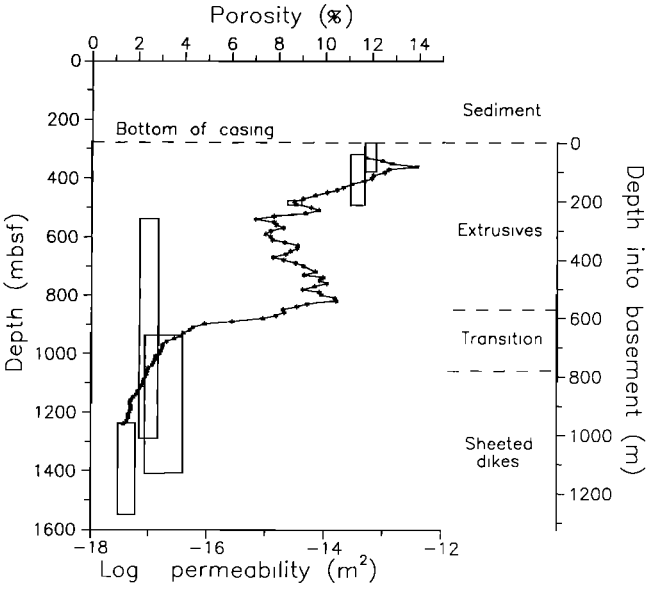

Fig. 14. Apparent bulk porosity and bulk permeabilities measured in DSDP hole 504B [*Becker*, 1985; *Anderson et al.*, 1985; *Becker et al.*, 1989]. With permeability values, the vertical extent of the rectangles represents the depth interval tested, while the horizontal extent represents estimated errors in individual measurements. The porosity and permeability units represented in the numerical models used in this study are listed in Table 5.

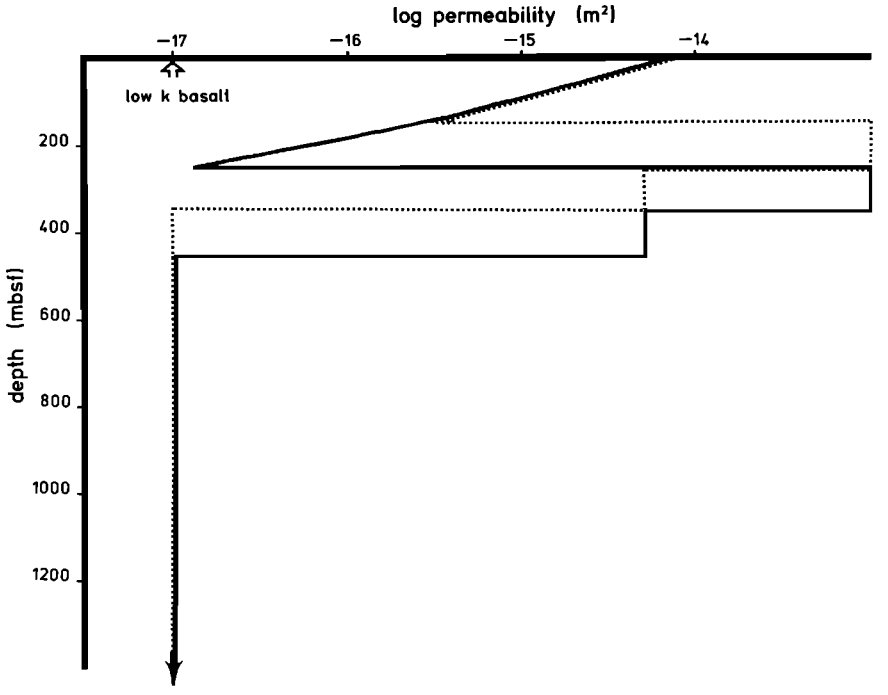

Fig. 15. The permeability/depth structures used in standard case tests in this study. The solid line indicates permeability versus depth in all standard simulations (for columns aligned with basement troughs in topographic simulations). The dotted line indicates permeability versus depth for columns aligned with basement ridges in topographic simulations (Tables 5 and 6). Permeability is high in shallow sediments, and then drops monotonically through to the sediment/crust contact (from about 10^{-14} to 10^{-17} m^2). Permeability jumps to 10^{-13} m^2 in the upper 100 m of basement, drops to 5×10^{-15} m^2 in the next 100 m, and then falls to 10^{-17} m^2 below the upper 200 m of basement. In tests with increased sediment permeabilities, these sediment values were increased by a factor of 10 or 100.

the upper basalt, and then steps down to the deep crustal value. Basalt grain density was fixed at 2900 kg m^{-3}. Matrix sediment and basalt were assigned specific heat values of 800 and 1300 kJ kg^{-1} K^{-1}, respectively. Parametric variations are listed in Table 6.

Results of Planar Simulations

The planar simulations tested the importance of parallel, layered heterogeneities in oceanic sediments and crust in directing fluid flow driven by buoyancy fluxes. Pertinent results are summarized in Tables 7 and 8.

The highest fluid velocities in all planar simulations are directed horizontally within the permeable basaltic layer. Velocities through the sediments are less than 0.01 mm yr^{-1} in standard case simulations but increase close to 1.0 mm yr^{-1} when sediment permeabilities are increased by a factor of 100 (Tables 6 and 7). The maximum underpressure dynamically maintained in the upper 200 m of basalt is 0.6 bar relative to cold hydrostatic and < 0.1 bar relative to hot hydrostatic. Pressure differences across the modeling domain at these depths are also < 0.1 bar. The combination of low pressure gradients (Table 8) and low permeabilities where $z > 450$ mbsf results in virtually no fluid movement in the lower crust. In the upper crust, a single convection cell formed with an aspect ratio of 20 (height, 500 m; length, 10 km)(Figure 16*a*).

Two separate simulations were run to determine the influence of the model dimensions on convection cell size and the applicability of vertical permeable, nonadiabatic boundary conditions. In the first simulation, each of the side boundaries was fixed with vertical temperature and hot hydrostatic pressure gradients [$T = T(z)$, $P = P(z)$], and at steady state, fluid everywhere inside of the modeled section became buoyant and exited through the top of the mesh, into the overlying ocean (Figure 16c). Both side boundaries became inexhaustible fluid sources, allowing recharge of this system from both low and high heat flow ends. Vertical pressure and temperature gradients are not held constant in the natural system but are in equilibrium with surrounding rock and fluid. In numerical simulations, however, the boundaries of the grid are also the boundaries of the flow domain; the material inside the model does not respond to conditions outside the model. Rather than adjusting the boundary gradients until a desired flow pattern was achieved, we doubled the domain width, from 10 to 20 km, and applied the standard impermeable, adiabatic boundary conditions.

The use of a 20-km-wide section allowed the innermost 10 km to communicate with the surrounding material and function in a more natural manner, with 5-km-wide buffers on either side. This simulation also tested whether the formation of a convection cell with an aspect ratio of about 20 was a favored mode in the model or if this geometry was strongly influenced by the positioning of impermeable boundaries. The resulting fluid flow pattern was identical to that in earlier simulations, except that the convection cell was doubled in width to 20 km, with an aspect ratio of 40. Fluid velocities and underpressures were virtually unchanged from the earlier, 10 km wide simulations.

In several simulations, only the upper 1500 m of oceanic sediment and crust were modeled, allowing the use of an extremely fine mesh (Figure 16*d*). These simulations included 10 sediment

TABLE 6. Key to Parametric Variations Simulated as Part of this Numerical Study

	Stage 1	Stage 2	Stage 3
Standard case	case 1	case 2	case 3
k_b (b_3) = 10^{-17} m^2 to z = 5 km	case 1PB		
Permeable side boundaries	case 1F		
Domain width 20 km	case 1W		
k_s increased by 100 ×	case 1PS	case 2PS	
k_s increased by 10 ×			case 3PS
k_b (b_1) increased by 10 ×			case 3PB

Stages 1 and 2 are planar tests (Figure 12); Stage 3 includes the topographic tests (Figure 13).

types, and most nodal elements had a thickness of just 25 m (Tables 4 and 5). This greater resolution allowed finer divisions between sediments with different physical properties and partially eliminated edge effects between elements with strong physical properties contrasts. Fluid velocities through sediments and basalt are little changed from those in more coarsely modeled domains (Table 7), except that the upper permeable section of basalt now contains a complete hydrothermal circulation cell, with an aspect ratio of about 40 (Figure 16*d*). It is easier for fluid to flow back along the high permeability conduit in the upper basalt than to flow up or down through the relatively impermeable overlying sediments or underlying basalt. This return flow probably did not appear in coarser simulations because of the more limited resolution (two 100-m layers versus eight 25-m layers).

In all planar simulations, the heat flow out through the top of the modeled section was little different from the heat input at the base, higher on the left side of the grid and lower on the right. Because velocities in the deep crust were low, fluid flow has little influence on heat transport in these cases.

The following summarizes results of and conclusions drawn from planar simulations:

1. Fluid flow velocities through the sediments were generally several orders of magnitude lower than those inferred to exist near site 504. In addition, nearly all fluid motion in the sediments was directed vertically; there was no significant horizontal fluid motion in the sediments.

2. Underpressures in the upper 200 m of basalt were less than 0.7 bar relative to cold hydrostatic and less than 0.1 bar relative to hot hydrostatic.

3. Convection in the crust below the upper 200 m occurred only at extremely low velocities and appeared to be insignificant in comparison to convection in the more permeable, shallow basalt. This was the case even when a permeability value of 10^{-17} m^2 was extended to the full 5 km depth of the oceanic crust. Thus deep crustal convection near site 504 is extremely unlikely and probably unimportant in terms of explaining the observations listed earlier.

4. The resolution in these simulations was important in determining the geometry of fluid flow. When depth resolution was increased, a complete convection cell formed in the upper, permeable basalt. Only a half cell formed in the more coarsely modeled simulations.

5. There is no tendency for subcritical convection cells to form with low aspect ratios, given a planar model and the background heat flow and permeability/depth structure apparent in the site 504 field area. Simulated circulation cells have aspect ratios of 20-40. The impermeable boundaries placed along the vertical edges of the simulation meshes appear to have determined the horizontal dimensions of the convection cells.

Results of Topographic/Sediment Drape Simulations

In these simulations, sediment thickness varied from 150 m over basement ridges to 250 m over basement troughs. Subdued seafloor bathymetry with an amplitude of 100 m and a wavelength of 4 km was created by draping sediment over basement with relief of 200 m at the same wavelength and phase (Figure 13), resulting in strong lateral gradients in pressure, temperature, and matrix permeability. The sediment/seawater interface was held at a constant temperature of 2.01°C, but hydrostatic pressure at this surface varied as a function of bathymetry. Basal heat input varied according to the same distribution as in planar simulations, and vertical boundaries were impermeable and adiabatic.

Sediment and basalt properties in these simulations were determined by the distance of each nodal center from the sediment/seawater interface, meaning that properties at any particular depth along a basement ridge were the same as those at the same depth beneath the seafloor along a trough. This

TABLE 7. Summary of Simulation Stability and Maximum Fluid Velocity Statistics

Test	ΔT_{max} °C	ΔP_{max} bar	max V_s mm yr-1			max V_b mm yr-1		
			Discharge	Recharge	Overall	b_1	b_2	b_3
Case 1	4.8 ×10-4	3.0 ×10-5	0.0034	0.0036	0.0034	0.078	0.022	0.0015
Case 1PB	1.2 ×10-3	6.4 ×10-4	0.078	0.079	0.078	0.25	0.016	0.029
Case 1PS	4.9 ×10-4	3.0 ×10-5	0.35	0.35	0.35	8.1	2.2	0.15
Case 2	4.2 ×10-12	9.1 ×10-11	0.0084	0.0084	0.0085	0.42	0.071	0.0055
Case 2PS	4.9 ×10-11	9.8 ×10-11	0.91	0.85	0.92	43	7.3	0.56
Case 3	5.7 ×10-11	5.0 ×10-11	1.9	1.7	1.9	12	1.5	0.0060
Case 3PS	1.9 ×10-11	1.2 ×10-8	11	5.9	18	36	5.8	0.17

ΔT_{max} and ΔP_{max} refer to the largest change in these variables in all nodes in the fluid flow domain over the last 2 × 10 5 year time step of each simulation. The extremely low values listed here indicate that near "steady-state" conditions have been achieved in all cases. V_s refers to fluid velocity in sediments while V_b is fluid velocity in basalt. In the V_s columns, "discharge" refers to fluid flow out of the sediments and into the overlying ocean, "recharge" is fluid flow into the sediments at the seafloor, and "overall" is fluid flow in any direction within the sediments. In the V_b columns, fluid velocities are listed for three basalt types, but not for any particular direction. This table is a companion to Figures 16 and 17.

Table 8. Listing of Pressure Differences Within Shallow Basalt Nodes in Planar Simulations

Test	Depth, mbsf	Basalt Type	ΔP_h, bars	ΔP_c, bars	ΔP_x, bars
Case 1	300	1	<0.1	0.3	<0.1
	400	2	<0.1	0.5	<0.1
Case 1PB	300	1	<0.1	0.3	<0.1
	400	2	<0.1	0.5	<0.1
Case 1PS	300	1	<0.1	0.3	<0.1
	400	2	<0.1	0.5	<0.1
Case 2	263	1	<0.1	0.2	<0.1
	288	1	<0.1	0.3	<0.1
	313	1	<0.1	0.3	<0.1
	338	1	<0.1	0.4	<0.1
	363	2	<0.1	0.4	<0.1
	388	2	<0.1	0.5	<0.1
	413	2	<0.1	0.6	<0.1
	438	2	<0.1	0.6	<0.1
Case 2PS	263	1	<0.1	0.2	<0.1
	288	1	<0.1	0.3	<0.1
	313	1	<0.1	0.3	<0.1
	338	1	<0.1	0.4	<0.1
	363	2	<0.1	0.4	<0.1
	388	2	<0.1	0.5	<0.1
	413	2	<0.1	0.6	<0.1
	438	2	<0.1	0.6	<0.1

Basalt type 1 has permeability of 10^{-13} m^2 while the permeability in basalt type 2 is 5×10^{-15} m^2. ΔP_h is the absolute value of the difference between in situ pressure the "hot" hydrostatic pressure appropriate for the same depth. ΔP_c is the absolute value of in situ pressure minus "cold" hydrostatic. Both of these are actually underpressures; the terms are explained in the text. ΔP_x refers to the pressure difference across the domain of the model. That $\Delta P_x < 0.1$ bar in all cases means that the listed ΔP_h and ΔP_c values also apply across the model domains. In fact, most ΔP_h and ΔP_c values were less than 0.001 bar, indicating that these planar tests resulted in little crustal convection. Contrast these results with those in Figure 18.

combination of bathymetry and differential sediment thickness in these simulations induces the formation of individual convection cells at one half the wavelength of the topographic variations (Figure 17). Fluid flows through the sediments at maximum rates of several to several tens of millimeters per year (Table 7). In addition, fluid flows up through the sediments over ridges and down through sediments over troughs. Fluid also flows laterally through the sediments between ridges and troughs. All these phenomena were inferred to exist in the site 504 field area [*Langseth and Mottl*, 1982; *CRRUST*, 1982; *Langseth et al.*, 1988; *Mottl*, 1989]. There are also significant differences between velocities of fluid discharge (over ridges) and recharge (over troughs). These velocity variations seem to be a response to variations in sediment thickness and hydraulic impedance. The overall convection geometry appears unaffected by differential sediment thickness, as fluids continue to flow down through the troughs, where hydraulic impedance is greatest (Figures 11 and 17).

Fluid flows through the upper basalt at velocities up to 36 mm yr^{-1} (Table 7), somewhat lower than suggested by *Langseth et al.* [1988]. Fluid velocities are greatly reduced in the lower, less permeable crust, as was predicted by *Lowell* [1980]. The convection cells induced in these simulations have an aspect ratio of about 5, but there is no evidence suggesting that longer cells with the same height could not be induced with proper topographic scaling. This result supports the assertion of *Hartline and Lister* [1981] that heat may travel laterally for long distances during topographically modified convection, although these authors argued that convection cell aspect ratios need not be large.

It is clear that the choice of adiabatic, impermeable vertical boundaries has little influence on cell geometry, as the fluid flow directions next to these boundaries are reversed from those in the planar simulations. For example, fluid flows down into the sediments adjacent to the left boundary in topographic simulations (Figure 17), while it flows up against this boundary in planar simulations (i.e., Figure 16*a*). The fluid flow direction at the boundaries is not strongly influenced by variations in basal heat flow either. Fluid flow velocities are virtually identical at equal depths and equivalent positions over all ridges and troughs; the vectors in Figure 17 have approximately the same orientation and magnitude at 2 km and 6 km from the left boundary. This simulated section of sediment and crust thus contains five convection cells. Only in these topographic simulations did more than one passive convection cell form in the 10-km-wide domain.

We were concerned that these simulations might be geochemically unrealistic if the total volume of fluid predicted to pass through the upper crust is sufficient to entirely strip the basalt of species such as Ca^{++}. Given a convection cell length of about 4 km, a permeable zone thickness of 200 m, basaltic porosity of 0.100-0.125, and steady state fluid flow velocities of the order of 5 to 50 mm yr^{-1}, however, it will take 500 ka to 5 Ma to acheive a water/rock ratio of 1 in the upper crust. With a typical abundance of CaO in oceanic basalts >10% [*Hekinian*, 1982], and a typical Ca^{++} concentration in upper basaltic pore fluids of 50-55 mmol [*Mottl et al.*, 1983*b*], it does not appear that seawater circulating through the upper crust near site 504 could leave this basalt stripped of Ca^{++} in only a few million years.

Simulated fluid underpressures in the upper 200 m of basalt are identical in positions of equal depth. A compilation of typical underpressures with respect to hot and cold hydrostatic is illustrated in Figure 18. Fluid underpressures on the flanks of the basement ridges vary between 2.6 and 10.8 bars, in good agreement with the value of 8 bars measured by *Anderson and Zoback* [1982] on the flank of a ridge in hole 504B. Interestingly, cold hydrostatic underpressures (Figure 18*a*) are close to hot hydrostatic values (Figure 18*b*); this was not the case in planar simulations, when simulated pressures were only marginally different from hot hydrostatic. Underpressures that are about the same relative to both hot and cold hydrostatic (as in these topographic simulations) are more likely to be long lived than are underpressures of the same magnitude relative to cold hydrostatic only.

Underpressures measured in a borehole on the seafloor are determined relative to a gradient which is somewhere between the hot and cold hydrostatic extremes. The drilling fluid used by the DSDP and ODP is seawater, which typically reaches a temperature near that of bottom water by the time it enters the borehole. Were a borehole to be drilled through the sediment and the upper crustal section that was modeled in planar simulations, the cold water flushing down the drill pipe would initially experience an underpressure relative to cold hydrostatic (≤0.6 bar; Table 8). After seawater was no longer pumped down the drill pipe, the fluids in the borehole would be warmed by the surrounding rock, and the water would experience an underpressure approaching hot hydrostatic (≤0.1 bar) as the mass of the borehole water column was reduced. This transition would be slowed by the drawdown of cold bottom water into the borehole and the underpressured formation.

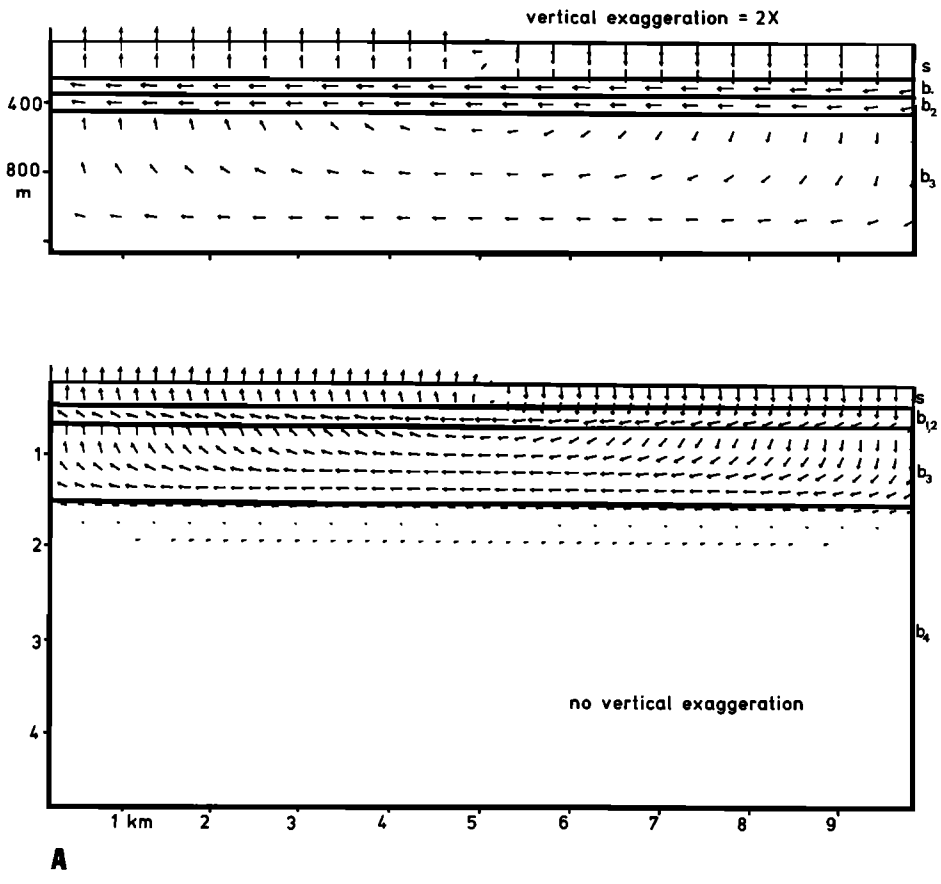

Fig. 16*a*. In this standard case, $k_b = 10^{-25}$ m^2 from 1500 to 5000 mbsf. Highest fluid velocity is 0.078 mm yr^{-1} in the shallow basalt. Fluid flow into and out of the sediments occurs at a maximum velocity of 0.0034 mm yr^{-1}. Note that flow along the shallow basalt is entirely right to left, from the low to the high heat flow ends of the modeled section. The lower half of a convection cell with an aspect ratio of about 20 has been created in the sediments and upper basalt. The highest velocity in the lower basalt is 0.0015 mm yr^{-1} (1.5 m m.y.$^{-1}$).

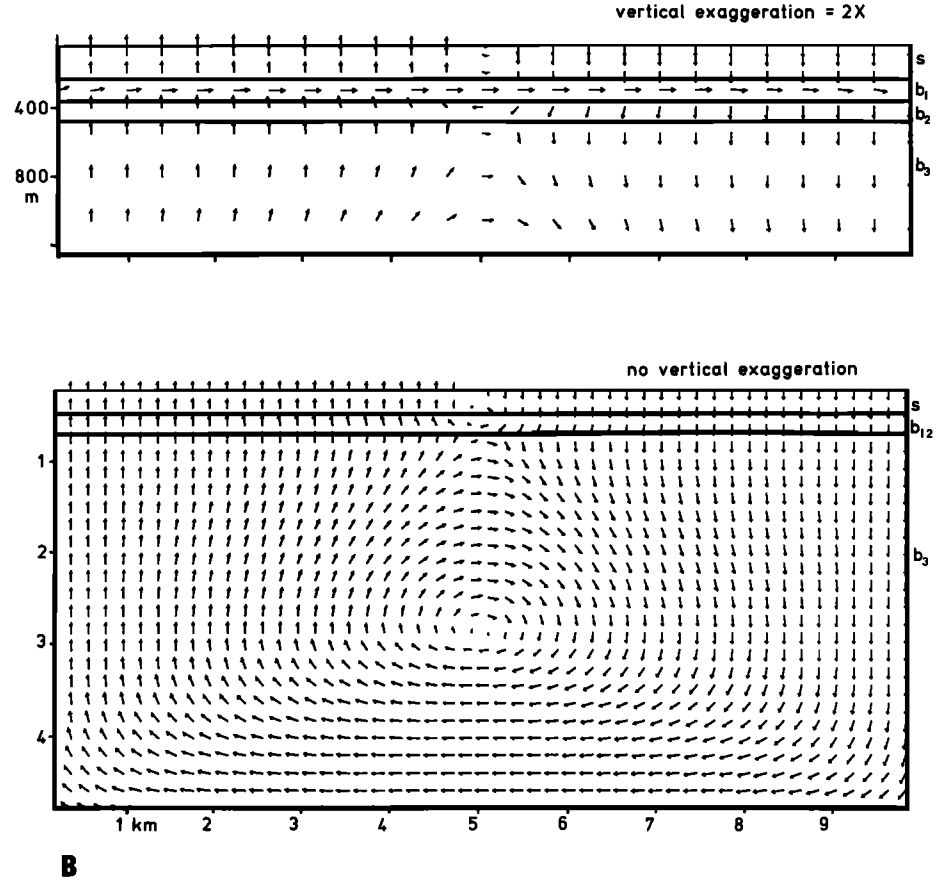

Fig 16*b*. In this permeable basalt case designed to examine the possibility of deep crustal convection, $k_b = 10^{-17}$ m^2 from 450 to 5000 mbsf. Note that fluid flow vectors within the most permeable basalt (b_1) have been "averaged" out in the lower diagram due to the interpolation scheme. In the upper diagram, net transport through this horizon is seen to be from left to right. The whole crust appears to be involved in convection, but at a maximum flow rate of just 0.029 mm yr^{-1} below the upper 200 m (Table 7). Fluid flow through the upper crust is in the opposite direction in comparison to the standard case in Figure 16*a*, because this horizon now contains the upper limb of a convection cell. Fluid velocities are somewhat higher through the sediments than in Figure 16*a*, but are still significantly lower than inferred by *Langseth et al.* [1988] (Table 7).

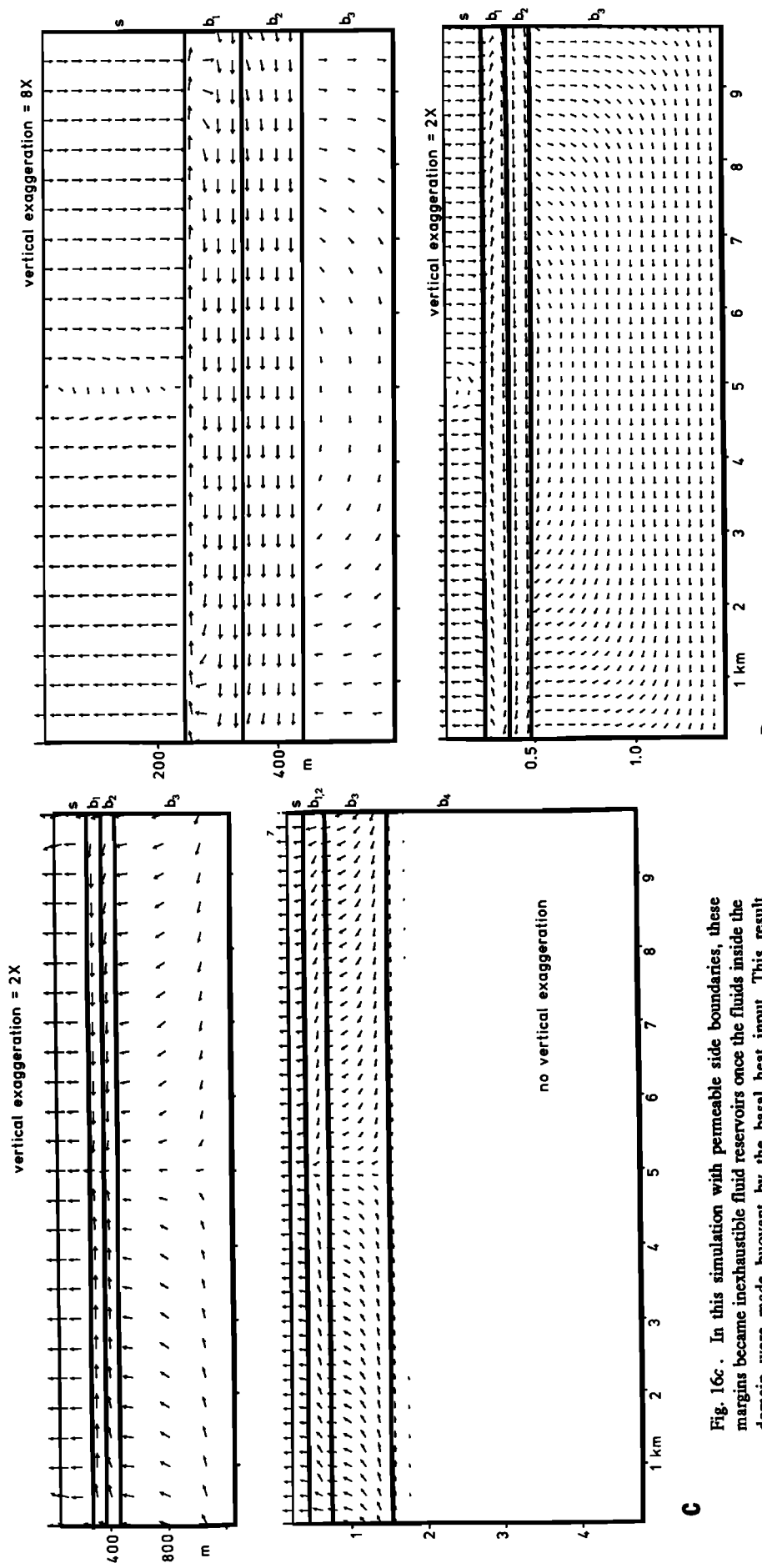

Fig. 16c. In this simulation with permeable side boundaries, these margins became inexhaustible fluid reservoirs once the fluids inside the domain were made buoyant by the basal heat input. This result demonstrates that the choice of vertical boundary conditions is crucial in determining fluid flow paths. In a separate test of boundary conditions, the model domain was doubled in width, and all other parameters were assumed the same as in the standard case in Figure 16*a* (Table 5). The resulting fluid flow vectors are identical to those in Figure 16*a*, except that the horizontal distances were doubled. This simulation provided a more realistic check on the use of permeable side boundaries and suggests that the choice of adiabatic, impermeable boundaries limits the length of simulated convection cells.

Fig. 16d. Stage 2 simulations modeled the upper 1500 m of sediments and crust at about 4 times the resolution of stage 1 simulations (Tables 4 and 5). A full convection cell with an aspect ratio of about 40 formed in the shallow basalt. Fluid flow velocities are virtually unchanged from those in the same portions of stage 1 tests. As in stage 1 tests, an increase in sediment permeabilities by a factor of 100 results in no change in fluid pressures (Table 8) but an increase in fluid velocities (Table 7). Note that both the lower and the upper diagrams are vertically exaggerated.

Fig. 16. Fluid flow vectors calculated for steady state planar simulations. Vectors are plotted on a log scale with a total maximum range of 10^{-17} to 10^{-10} m s^{-1}. The lower diagram in each pair illustrates fluid flow over the entire modeling domain, after the unevenly scattered vectors have been redistributed [*Akima*, 1978]. This redistribution tends to smooth out contrasts in fluid flow, particularly between materials with strongly different permeabilities. The upper diagrams illustrate the shallowest portions of the modeled domains, with vectors plotted in their actual positions directly over the center of individual mesh elements. Model configurations and physical properties are summarized in Tables 4-6. Maximum fluid velocities in individual portions of the model domains are listed in Table 7.

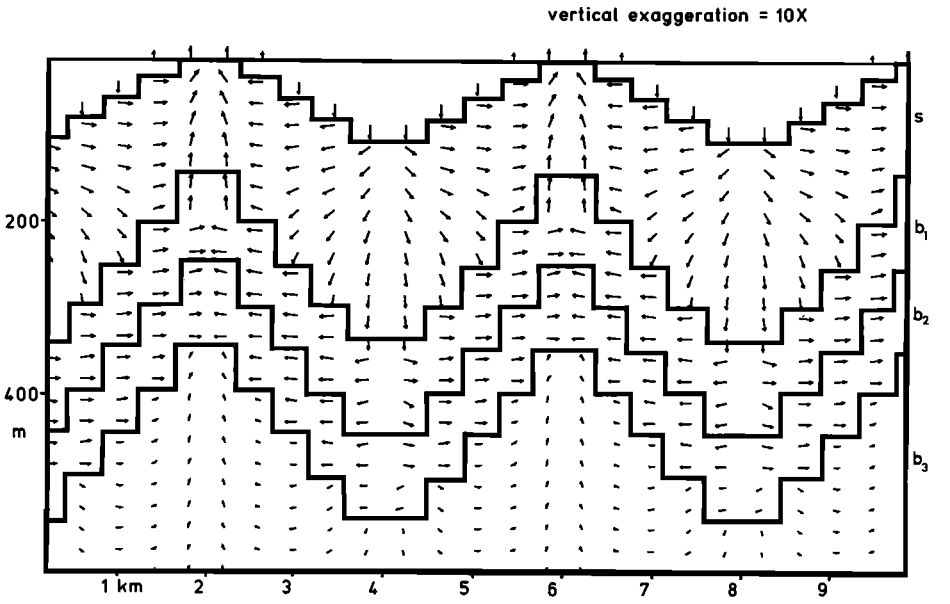

Fig. 17. Fluid flow vectors calculated for a steady state topographic simulation with standard physical properties. Vectors are plotted on a log scale with a total maximum range of 10^{-15} to 10^{-8} m s^{-1}. This diagram illustrates the upper portion of the modeled domain, with vectors plotted in their actual positions directly over the center of individual elements. Note that fluid flows vertically and laterally through sediments and underlying permeable basalt. The model configuration and sediment and basalt physical properties are summarized in Tables 4-6. Maximum fluid velocities in individual portions of the modeling domain are listed in Table 7. An increase in sediment permeabilities by a factor of 10 (Table 6) increased fluid velocities (Table 7) but had little influence on convection geometry.

The underpressures relative to both cold and hot hydrostatic predicted during topographic simulations are significantly higher than those in planar simulations (compare Figure 18 and Table 8). Fluid flow velocities within the crust were low in planar simulations because pore pressures were only marginally different from hot hydrostatic; strong underpressures relative to hot hydrostatic in the oceanic crust draw fluids through the sediments from the overlying ocean and drive passive hydrothermal circulation. However, it was the cold hydrostatic underpressure that drove seawater into the upper basement in hole 504B immediately after the sediment seal was punctured. Since the hydrostatic underpressure in a borehole should be expected to move from cold hydrostatic towards hot hydrostatic with time, assuming that drawdown is not so rapid and long-lived as to prevent warming of the borehole fluid entirely, the intensity of fluid draw-down will depend at first on (1) the initial (cold hydrostatic) underpressure, and much later, on (2) the difference between cold and hot hydrostatic gradients. The underpressures in these topographic simulations result from the heating of pore fluids in combination with a static geometry; the lower underpressures in planar simulations were purely dynamic.

The actual underpressure in hole 504B has persisted, although at a reduced level, over the 7 years between leg 69 and leg 111. These topographic simulations reasonably duplicate the initial underpressure in hole 504B and also explain why this underpressure was so long-lived: the transition from a cold hydrostatic to a hot hydrostatic state around the borehole results in little change in underpressuring (Figure 18). These simulations also suggest that the hot hydrostatic underpressures, which result from the natural heat flow and geometry of the crust/sediment system, should have allowed for continued drawdown into hole 504B between legs 69 and 111, assuming that the permeability in the upper 200 m of crust was not degraded. The observation that the flow rate into hole 504B has been reduced by about 99% during this time [*Gable et al.*, 1989] suggests that if the "reservoir" concept for the permeable basalt surrounding hole 504B is valid, then the reservoir may be of limited extent [e.g., *Becker et al.*, 1983*b*; 1989]. The idea that a portion of the oceanic crust acts as a reservoir is a conceptual artifact, of course, as we do not know where the fluid drawn into hole 504B has gone. These results complement those of *Williams et al.* [1986], who reasonably predicted the formation of basement underpressures after several million years of sedimentation, and the resulting fluid draw down after drilling in hole 504B.

A comparison of heat flow values predicted by the various topographic simulations (Figure 19) suggests that the topographic model can largely explain differences in heat flow around site 504, the correlation between heat flow, bathymetry, sediment thickness and geochemical gradients, and the tendancy for the heat flow lows to be broad while heat flow highs are narrow. Heat flow is increased over bathymetric and basement ridges due to two effects in these simulations, the upward motion of pore fluids through the sediment column, and partial equalization of temperatures at the sediment/basement interface. In the natural system, the first effect appears to be the less important of the two. The latter effect results from the rapid, lateral flow of fluids along the permeable section of upper crust.

Under purely conductive conditions, heat flow at the seafloor tends to be higher over bathymetric troughs due to refraction [*Lachenbruch*, 1968]. During topographic simulations, heat flow is increased over the ridges, with a total amplitude in heat flow variations up to 40 mW m^{-2}. This variation is appropriate around site 504, where the standard deviation in heat flow is about 36 mW m^{-2} (Figure 5). In addition, the zones of high heat flow are

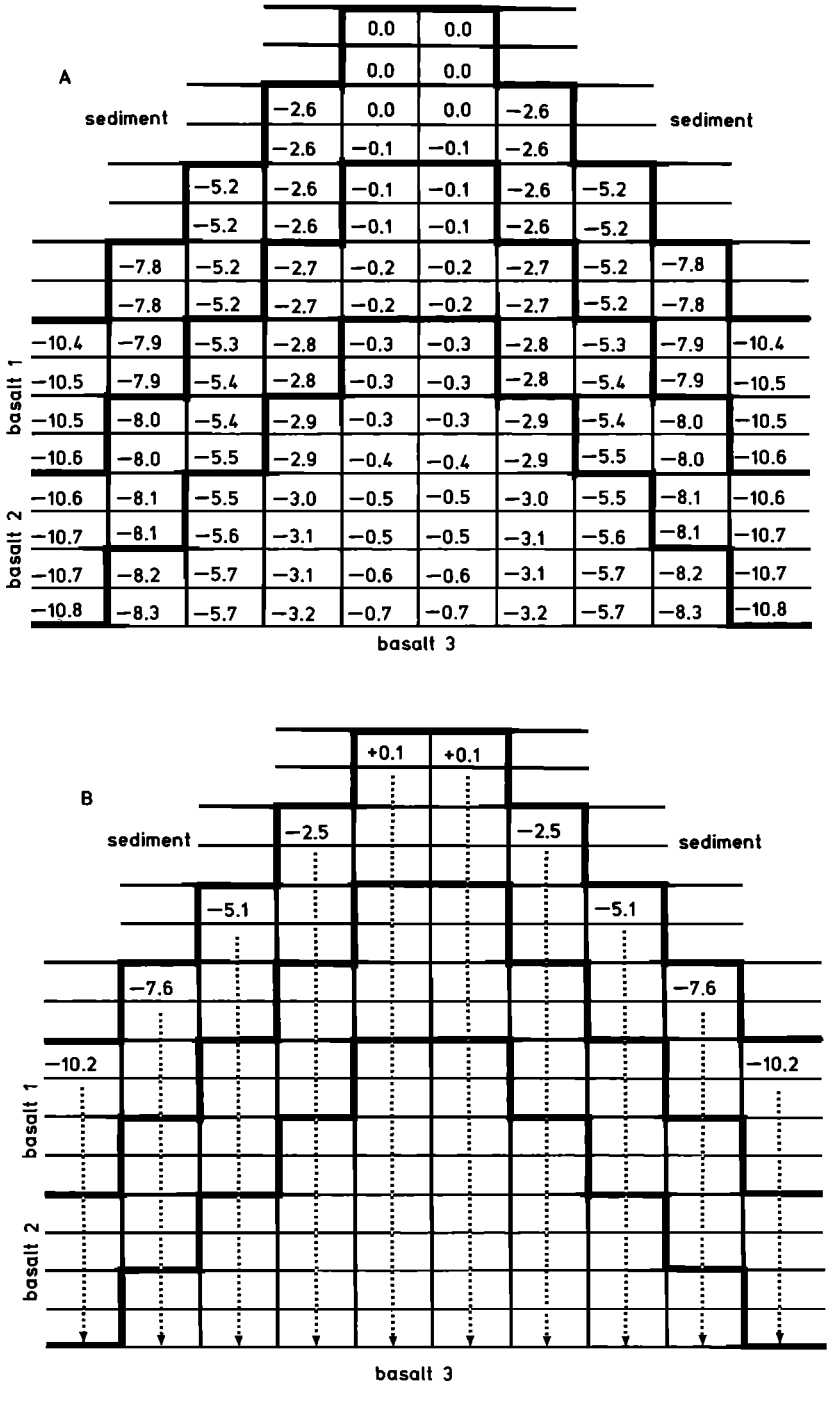

Fig. 18. ΔP (calculated pressure minus hydrostatic) for each element in upper basalt in topographic simulations. The portion of the modeling domain represented in these diagrams corresponds to any trough-ridge-trough set in Figures 13 and 17. Underpressures are symmetrically distributed about the peaks of the ridges and vary as a function of depth only. The distinction between hot and cold hydrostatic gradients is explained in the text. (*a*) ΔP_c: calculated pressure versus cold hydrostatic. (*b*) ΔP_h: calculated pressure versus hot hydrostatic.

relatively narrow and deviate most strongly from the mean, while the zones of lower heat flow are broader and contain values closer to the mean (compare Figures 6 and 19).

In order to acheive a better fit between heat flow in these simulations and in the natural system, it was necessary to increase the permeability in the upper 50 m of basalt to 10^{-12} m^2 (Figure 19). Although measurements of bulk permeability in the upper 100-200 m of basalt surrounding hole 504B indicate an average value of about 10^{-13} m^2 [*Anderson and Zoback*, 1982], it is not immediately clear how this permeability is distributed. *Becker et al.* [1983*a*] originally suggested that the most permeable section surrounding the borehole may be a relatively narrow zone, several tens of meters in thickness, with somewhat lower permeability in the remaining portion of the upper 200 m of crust. It was not possible to test the effects of increasing permeability in an even thinner layer in the upper basement (i.e., 10-20 m) because of

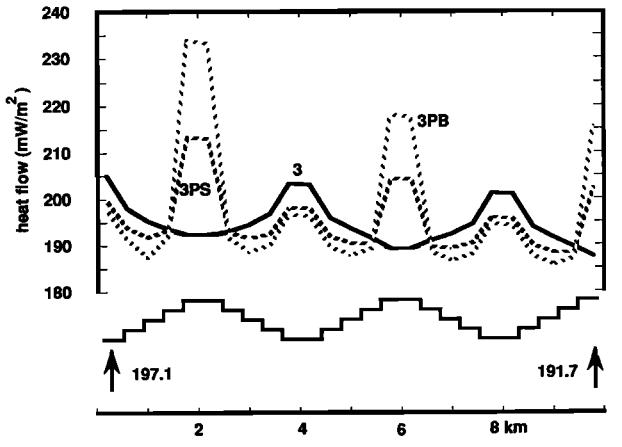

Fig. 19. Heat flow through the top of three topographic simulations. Seafloor bathymetry is indicated schematically in the lower half of the figure. The basal heat input varies linearly from 197.1 mW m-2 on the left side of the domain to 191.7 mW m-2 on the right side. The three curves indicate combined conductive and advective heat flow in each of three parametric variations. Case 3; standard physical properties. Note that the heat output is highest in the troughs and lowest over ridges, in contrast to field observations, due to refraction at the seafloor. Case 3PS; Sediment permeabilities increased everywhere over those in case 3 by a factor of 10. Fluid velocities have been increased both in the sediments and through the upper basalt (Table 7). Case 3PB; permeability in the upper 50 m of basement increased over that in case 3 by a factor of 10. The amplitude of the heat flow variations in case 3PB is about 40 mW m2, approximately equal to the standard deviation in heat flow values around site 504 (Figure 5). Heat flow in these simulations is still somewhat raised in bathymetric troughs, due to refraction at the seafloor. In order to better match field observations it will be necessary to further equalize temperatures at the sediment/basement interface. Even in case 3PB, the temperatures at the interface on ridges are about 15°C lower than the temperatures at the interface in troughs.

geometrical and computational constraints in the numerical model.

There are several possible reasons why variations in heat flow of up to 100%, as seen around site 504 [Langseth et al., 1988], were not duplicated in these simulations. First, the variation in sediment thickness included in the simulations was 150-250 m, as required in order to allow fine scaling in the numerical model, rather than the 140-310 m variation which may exist around site 504 (Figure 14). Second, temperatures at the sediment/basement interface were only partly homogenized (by about 25%) during these simulations. The stepwise representation of topgraphic relief in the model (Figure 13) required that the path through which fluids traveled in the upper crust was extremely tortuous. Since the model requires that fluids and the surrounding matrix be at thermal equilibrium, the transport of heat in the simulations may be considerably less efficient than in the natural system, particularly in directions other than purely horizontal or purely vertical. Also, as the pressure differences between the upper basalt and the seafloor are largely fixed by the geometry of the system, the hydraulic impedance of the sediment layer limits the maximum mass of fluid that can be pumped through the system over a given time. Were there to be a thin zone of even higher permeability in the upper crust, it would be possible to move the same fluid mass through this zone at a much higher velocity than seen in the shallow basalt in these simulations. The faster the fluid moves up the flanks of the ridges, the more efficient it will be in transporting heat and equalizing temperatures at the sediment/basement interface. Still, the general trends of the heat flow distribution around site 504 have been duplicated in these simulations.

Results of these topographic simulations are summarized as follows:

1. There is a tendency for subcritical convection cells to form in laterally and vertically heterogeneous sediment and crust with a cell length equal to one half the wavelength of topographic variations. Convection is stable in a model system designed to include physical properties and boundary conditions appropriate near site 504.

2. Once convection cells are induced, sediment thickness and resulting variations in hydraulic impedance alter fluid velocities through the sediments but have little effect on overall geometry. The cell geometry is determined by the wavelength of topography and the depth to the base of relatively permeable basalt. There does not appear to be any favored aspect ratio for subcritical convection under these conditions.

3. The impermeable boundaries placed along the vertical edges of the flow domains appear to have little influence on the geometry of topographically induced convection cells.

4. Velocities of fluid flow through sediments and basalt are comparable to those appropriate for the site 504 field area, as inferred from geochemical and geothermal data.

5. Lateral fluid flow through the sediments, a process not seen in any planar model, is induced by topographic variations. It appears that significant topography is required to establish and maintain lateral pressure gradients sufficiently strong to drive subhorizontal fluid flow through thick sediments.

6. The geometry of topographically induced fluid flow on the southern flank of the CRR is not strongly affected by lateral variations in basal heat input.

7. The combination of basal heat input, basement topography and uneven sediment drape combine to create underpressures in the upper basement of the order of several to 10 bars, relative to both cold and hot hydrostatic pressure gradients. Except at the top of basement ridges, the upper crust is underpressured everywhere in these simulations.

8. Whole crustal convection is not required to explain dynamically maintained fluid flow and underpressures in basement. It is possible that only the upper several hundred meters of crust is significantly involved.

9. The general distribution in heat flow around site 504 appears to be satisfied by this model. While temperatures in the upper crust have not been entirely equalized (as was assumed in the conductive analysis of heat flow variations presented earlier in this paper), this numerical result may be due, in part, to geometrical restrictions in the simulations.

CONCLUSIONS

A wide variety of geological, geophysical, and geochemical observations appear to result from basement relief with an amplitude of several hundred meters and a wavelength of several kilometers. Sediment is thicker in basement troughs and thinner over ridges as a result of ordinary depositional processes on an uneven surface. Thick and thin sediments which are bounded on the top and bottom by near-isothermal surfaces, may result in significant variations in surface heat flow, despite relatively uniform input at the base of the crust. This same relief, in combination with the buoyancy flux induced by the basal heat input, establishes lateral and vertical pressure and temperature gradients, sustaining passive, subcritical convection through

sediments and crust, and multibar underpressures in portions of upper basement. This circulation may provide a mechanism for largely homogenizing the temperatures and geochemistry of pore fluids near the sediment-basalt interface. The positive correlation between surface heat flow, geochemical gradients, and sediment thickness [*Langseth et al.* 1988] may thus result not because fluid flow through the sediments significantly alters heat flow, but because heat and fluid flow anomalies result from the same mechanism, variations in basement topography. We do not argue that the geometry of fluid convection is strictly two-dimensional; rather, two-dimensional simulations have been used to demonstrate that the combination of basal heat input and basement topography provide variations in heat flow, fluid flow and basement pore pressures which are appropriate for this setting. The actual geometry of fluid flow is probably three-dimensional.

If this conceptual model is correct, with the dimensions of convection cells determined by the length scale of bathymetry, then these cells would tend to be rafted along with the spreading plate, as suggested by *Fehn and Cathles* [1979, 1986] and *Fehn et al.* [1983]. In addition, once topographic effects dominate convection geometry off axis, upflow and downflow zones will remain fixed relative to the crust until continued sedimentation and the infilling of cracks and pores block fluid movement. This finding is consistent with observations from DSDP hole 395 [*Lawrence and Drever*, 1981], hole 418A [*Hart and Staudigel*, 1979], and many others (see discussion of *Fehn and Cathles* [1986]) which show strong evidence of long-term, low-temperature alteration resulting from the penetration of cold seawater. *Fehn and Cathles* [1986] attributed the bias in sampling toward crustal recharge zones to drilling in well-sedimented basins, as opposed to thinly sedimented ridges. Also, upflow in these passive systems does tend to be more concentrated laterally than recharge [*Fehn et al.*, 1983].

The movement of convection cells in our simulations is not a direct result of heat being advected laterally with the moving plate, but results instead from the interaction of heat-induced buoyancy fluxes and the presence of lateral pressure and temperature gradients maintained by isothermal, nonisobaric boundaries at the seafloor and between sediments and crust. This topographic forcing modifies the intensity and geometry of passive convection on the ridge flank. The underpressures which result from this combination of heat input and geometry are not the dynamic result of passive convection; instead the convection results from variations in underpressures, which themselves require a particular system geometry.

Fehn and Cathles [1986] presented two end- members to the spectrum of possible permeability structures in the oceanic crust, one with a porous media distribution which is constant laterally (as in their models) and the other in which fluid flow is confined to widely spaced, discrete fractures. Our simulations suggest that near site 504, the permeability structure may be modification of the first end-member, in which lateral variations are included in a porous media representation. A more realistic simulation might include appropriate three-dimensional topography plus fractures or faults, perhaps separating basement troughs and ridges.

NOTATION

A area [L^2].
c_f volume specific heat (fluid) [energy L^{-3} deg^{-1}].
e void ratio.
e_f internal energy (fluid) [energy M^{-1}].
$\mathbf{g}$ gravitational acceleration [$L\,T^{-2}$].
h thickness of a sediment layer [L].
H thickness of a porous medium [L].
I hydraulic impedence [L^{-1}].
k absolute permeability [L^2].
$\mathbf{n}$ unit outer normal.
P fluid pressure [$M\,L^{-1}\,T^{-2}$].
ΔP_c differential pressure versus cold hydrostatic [$M\,L^{-1}\,T^{-2}$].
ΔP_h differential pressure versus hot hydrostatic [$M\,L^{-1}\,T^{-2}$].
ΔP_x differential pressure across model domain [$M\,L^{-1}\,T^{-2}$].
R_a Rayleigh number.
R_c critical Rayleigh number.
t time [T].
T temperature [deg].
V volume [L^3].
v_d darcy velocity [L T^{-1}].
w vertical fluid velocity [L T^{-1}].
x horizontal distance [L].
z depth beneath seafloor [L].
α fluid thermal expansivity [L deg^{-1}].
β compressibility [$L\,T^2\,M^{-1}$].
γ thermal gradient [deg L^{-1}].
ϕ porosity.
λ thermal conductivity [energy $L^{-1}\,T^{-1}$ deg^{-1}].
μ dynamic viscosity [$M\,L^{-1}\,T^{-1}$].
υ kinematic viscosity [$L^2\,T^{-1}$].
ρ density [$M\,L^{-3}$].
ζ convection cell aspect ratio (length/depth).
ξ wavenumber [L^{-1}].

Acknowledgments. This research was supported by the Koczy Fellowship, administered through the Rosenstiel School of Marine and Atmospheric Science, University of Miami, and National Science Foundation grants OCE85-17013, OCE86-08261, OCE85-16773, and OCE88-00077. This manuscript benefited from discussions with C. G. A. Harrison, D. Olson, C. Rooth, and J. Southam, and thoughtful reviews by N. Sleep and R. P. Von Herzen.

REFERENCES

Akima, H., A method of bivariate interpolation and smooth surface fitting for irregularly distributed data points, *ACM Trans. Math. Software, 4*, 148-159, 1978.

Alt, J. C., J. Honnorez, C. Laverne, and R. Emmermann, Hydrothermal alteration of a 1-km section through the upper oceanic crust, Deep Sea Drilling Project hole 504B, mineralogy, chemistry and evolution of seawater-basalt interactions, *J. Geophys. Res., 91*, 10,309-10,335, 1986.

Anderson, R., and M. Hobart, The relation between heat flow, sediment thickness, and age in the Eastern Pacific, *J. Geophys. Res., 81*, 2968-2989, 1976.

Anderson, R. N., and M. D. Zoback, Permeability, underpressures and convection in the oceanic crust near the Costa Rica Rift, eastern equatorial Pacific, *J. Geophys. Res., 87*, 2860-2868, 1982.

Anderson, R., M. G. Langseth, and J. Sclater, The mechanisms of heat transfer through the floor of the Indian Ocean, *J. Geophys. Res., 82*, 3391-3409, 1977.

Anderson, R. N., M. D. Zoback, S. H. Hickman, and R. L. Newmark, Permeability versus depth in the upper oceanic crust, in situ measurements in Deep Sea Drilling Project hole 504B, eastern equatorial Pacific, *J. Geophys. Res., 90*, 3659-3669, 1985.

Becker, K., Large scale electrical resistivity and bulk porosity of the oceanic crust, *Initial Rep. Deep Sea Drill. Proj., 83*, 410-428, 1985.

Becker, K., Hydrogeology of young oceanic crust, downhole experiments in ODP holes 395A, 504B and 735B, *Eos Trans. AGU, 69*, 1402, 1988.

Becker, K., Measurements of the permeability of the sheeted dikes in hole 504B, ODP leg 111, in K. Becker and H. Sakai, *Proceedings of ODP Scientific Results*, vol. 111, Ocean Drilling Program, College Station, TX, in press, 1989.

Becker, K., M. G. Langseth, and R. D. Hyndman, Temperature measurements in hole 395A, leg 78B, *Initial Rep. Deep Sea Drill. Proj., 78B*, 689-698, 1984.

Becker, K., M. G. Langseth, and R. P. Von Herzen, Deep crustal geothermal measurements, hole 504B, Deep Sea Drilling Project legs 69 and 70, *Initial Rep. Deep Sea Drill. Proj., 69*, 223-236, 1983*a*.

Becker, K., M. Langseth, R. Von Herzen, and R. Anderson, Deep crustal geothermal measurements, hole 504B, Costa Rica Rift, *J. Geophys. Res., 88*, 3447-3457, 1983*b*.

Becker, K., M. Langseth, R. Von Herzen, R. Anderson, and M. Hobart, Deep crustal geothermal measurements, hole 504B, Costa Rica Rift, legs 69, 70, 83, and 92, *Initial Rep. Deep Sea Drill. Proj., 83*, 405-418, 1985.

Becker, K., et al., *Proceeding ODP, Initial Reports*, vol. 111, College Station, TX (Ocean Drilling Program), 1988.

Becker, K., et al., Deep drilling into young oceanic crust, hole 504B, Costa Rica Rift, *Rev. Geophys., 27*, 79-102, 1989.

Bischoff, J. L., and R. J. Rosenbauer, The critical point and two-phase boundary of seawater, 200°C-500°C, *Earth Plant. Sci. Lett., 68*, 172-180, 1984..

Bischoff, J. L., and R. J. Rosenbauer, An equation of state for hydrothermal seawater (3.2 percent NaCl), *Am. J. Sci., 285*, 725-763, 1985.

Bodvarsson, G. S., Mathematical modeling of the behavior of geothermal systems under exploitation, Ph. D. thesis, 353 pp., Univ. of Calif., Berkeley, 1982.

Bredehoeft, J. D., and I. S. Papadopulos, Rates of vertical groundwater movement estimated from the earth's thermal profile, *Water Resour. Res.*, 2, 235-328, 1965.

Brocher, T. M., E. L. Geist, J. A. Collins, and J. C. Mutter, 1986, Seismic structure of the oceanic crust in the vicinity of DSDP site 504, *Eos Trans. AGU, 67*, 1083, 1986.

Bryant, W. R., A. P. Delflanche, and P . H. Trabant, Consolidation of marine clays and carbonates, in *Deep-Sea Sediments, Physical and Mechanical Properties*, edited by A. L. Inderbitzen, pp. 209-244, Plenum, New York, 1974.

Campbell, A. C., T. S. Bowers, C. I. Measures, K. K. Faulkner, M. Khadem, and J. M. Edmond, A time series of vent fluid composotions from 21° N, East Pacific Rise (1979, 1981, 1985) and the Guaymas Basin, Gulf of California (1982, 1985), *J. Geophys. Res., 93*, 4537-4549, 1988.

Cann, J., et al., 1983, *Initial Reports Deep Ses Drilling Project 69*, (U.S. Govt. Printing Office), Washington, D.C., 1983.

Carnahan, B., H. A. Luther, and J. O. Wilkes, *Applied Numerical Methods*, John Wiley, New York, 604 pp., 1969.

Costa Rica Rift United Scientific Team, Geothermal regimes of the Costa Rica Rift, east Pacific, investigated by drilling, DSDP-IPOD legs 68, 69 and 70, *Bull. Geol. Soc. Am., 93*, 862-875, 1982.

Cowan, J. and J. Cann, Supercritical two-phase separation of hydrothermal fluids in the Troodos ophiolite, *Nature, 333*, 259-261, 1988.

Embley, R., M. Hobart, R. Anderson, and D. Abbot, Anomalous heat flow in the northwest Atlantic, a case for continued hydrothermal circulation in 80 MY crust, *J. Geophys. Res., 88*, 1067-1074, 1983.

Fehn, U., and L. Cathles, Hydrothermal convection at slow-spreading midocean ridges, *Tectonophysics, 55*, 239-260, 1979.

Fehn, U., and L. Cathles, The influence of plate movement on the evolution of hydrothermal convection cells in the oceanic crust, *Tectonophysics, 125*, 289-312, 1986.

Fehn, U., K. Green, R. Von Herzen, and L. Cathles, Numerical models for the hydrothermal field at the Galapagos Spreading Center, *J. Geophys. Res., 88*, 1033-1048, 1983.

Fisher, A. T., Heat flow and hydrothermal circulation through young oceanic sediments and crust, Ph.D. thesis, Univ. of Miami, Miami, FL, 235 pp, 1989.

Fyfe, W. S. and P. Lonsdale, Hydrothermal activity, *The Sea*, vol. 7, edited by C. Emiliani, pp. 589-638, John Wiley, New York, 1981.

Gable, R., R. Morin, and K. Becker, the geothermal state of hole 504B, ODP leg 111 overview, *Proceedings of ODP Scientific Results*, vol. 111, edited by K. Becker and H.Sakai, Ocean Drilling Program, College Station, TX, in press, 1989.

Goldfarb, M. S., and J. R. Delaney, Response of two-phase fluids to fracture configurations within submarine hydrothermal systems, *J. Geophys. Res., 93*, 4585-4594, 1988.

Green, K., Geothermal processes at the Galapagos Spreading Center, Ph.D. thesis, Mass. Inst. of Technol./Woods Hole Oceanogr. Inst., Woods Hole, 1980.

Gregory, R. T. and H. P. Taylor, An oxygen isotope profile in a section of Cretaceous oceanic crust, Samail ophiolite, Oman, evidence for $\delta^{18}O$ buffering of the oceans by deep (>5 km) seawater-hydrothermal circulation at mid-ocean ridges, *J. Geophys. Res., 86*, 2737-2755, 1981.

Haar, L., J. S. Gallagher, and G. S. Kell, *NBS/NRC Steam Tables*, 316 pp., Hemisphere, Washington, D. C., 1984.

Hamilton, E. L ., Variations in density and porosity with depth in deep-sea sediments, *J. Sediment Petrol., 46*, 280-300, 1976.

Hart, S. R. and H. Staudigel, Ocean crust-seawater interactions, sites 417 and 418,, *Initial Reports Deep Sea Drill. Proj., 51, 52, 53*, part 2, 1169-1176, 1979.

Hartline, B. K., and C. R. B. Lister, Topographic forcing of supercritical convection in a porous medium such as the oceanic crust, *Earth Planet. Sci. Lett., 55*, 75-86, 1981.

Hekinian, R., *Petrology of the Ocean Floor*, 393 pp., Elsevier, New York, 1982.

Hobart, M., M. Langseth, and R. Anderson, A geothermal and geophysical survey of the south flank of the Costa Rica Rift, sites 504 and 505, *Initial Reports Deep Sea Drill. Proj., 83*, 379-404, 1985.

Hyndman, R. D., R. P. Von Herzen, A. J. Erickson, and J. Jolivet, Heat flow measurements in deep crustal holes on the Mid, 1976-Atlantic Ridge, *J. Geophys. Res., 81*, 4053-4060.

Javandal, I., C. Doughty and C. F. Tsang, *Groundwater Transport, Handbook of Numerical Models, Water Resour. Monogr.*, vol. 10, 228pp., AGU, Washington, D. C., 1984.

Karato, S., and K. Becker, Porosity and hydraulic properties of sediments from the Galapagos Spreading Center and their relation to hydrothermal circulation in the oceanic crust, *J. Geophys. Res., 88*, 1009-1017, 1983.

Kastner, M., J. M. Gieskes, and J.-Y. Hu, Carbonate recrystalization in basal sediments, evidence for convective flow on a ridge flank, *Nature, 321*, 158-161, 1986.

Keenan, J. H. et al., *Steam Tables*, John Wiley, New York, 1969.

Kestin, J., Thermal conductivity of water and steam, *Mech. Eng., 100*, 46-48, 1978.

Lachenbruch, A., Rapid estimation of the topographic disturbance to superficial thermal gradients, *Rev. Geophys., 6* , 365-400, 1968.

Langseth, M., and B. Herman, Heat transfer in the oceanic crust of the Brazil Basin, *J. Geophys. Res. 86*, 10,805-10,819, 1981.

Langseth, M. and M. Mottl, Geochemical and geothermal mapping of crustal circulation patterns near Deep Sea Drilling Project sites 501/504, *Eos Trans. AGU, 63*, 1116, 1982.

Langseth, M., J. Cann, J. Natland, and M. Hobart, Geothermal phenomena at the Costa Rica Rift, background to objectives for drilling at Deep Sea Drilling Project sites 501, 504, and 505, *Initial Reports Deep Sea Drill. Proj., 69*, 5-29, 1983.

Langseth, M. G., M. J. Mottl, M. A. Hobart, and A. T. Fisher, The distribution of geothermal and geochemical gradients near site 501/504, implications for hydrothermal circulation in the oceanic crust, *Proceedings of ODP Initial Reports*, vol. 111, 23-32, edited by K. Becker and H. Sakai, Ocean Drilling Program, College Station, TX, 1988.

Lapwood, E., Convection of a fluid in a porous media, *Proc. Cambridge Philos. Soc., 44*, 508-521, 1948.

Lawrence, J. G., and J. I. Drever, Evidence for cold water circulation at DSDP site 395, isotopes and chemistry of alteration products, *J. Geophys. Res., 86*, 5125-5133, 1981.

Lawrence, J. R., and J. Gieskes, Constraints on water transport and alteration in the oceanic crust from the isotopic composition of pore water, *J. Geophys. Res., 86*, 7924-7934, 1981.

Lawrence, J. R., J. Gieskes, and W. Broecker, Oxygen isotope and cation composition of DSDP pore waters and the alteration of layer II basalts, *Earth Planet. Sci. Lett., 27*, 1-10, 1975.

Leinen, M., et al., Advection in the east Pacific, *Nature, 304*, 16, 1983.

Lister, C. R. B., On the thermal balance of a mid ocean ridge, *Geophys. J. R. Astron. Soc., 26*, 515-535, 1972.

Lister, C. R. B., On the penetration of water into hot rock, *Geophys. J. R. Astro. Soc., 39*, 465-509, 1974.

Lister, C. R. B., Active and passive hydrothermal systems in the oceanic crust, predicted physical conditions, in *The dynamic environment of the ocean floor*, edited by K. A. Fanning and F. T. Manheim, p. 441-470, D. C. Heath, Lexington, Mass., 1981.

Lonsdale, P., Deep tow observations at the mounds abyssal hydrothermal field, Galapagos Rift, *Earth. Planet. Sci. Lett., 36*, 92-110, 1977.

Lonsdale, P., and K. D. Klitgord, Structure and tectonic history of the eastern Panama Basin, *Geol. Soc. Am. Bull., 89*, 981-999, 1978.

Lowell, R. P., Topographically driven subcritical hydrothermal convection in the oceanic crust, *Earth Planet. Sci. Lett., 49*, 21-28, 1980.

Mangold, D. C., and C.-F. Tsang, Summary of hydrologic and hydrochemical models with potential application to deep underground injection performance, *Rep. LBL-23497*, 54 pp., Lawrence Berkeley Laboratory, Berkeley, Calif., 1987.

Maris, C., and M. Bender, Upwelling of hydrothermal solutions through ridge flank sediments shown by porewater profiles, *Science, 216*, 623-626, 1982.

Morin, R., and A. J. Silva, The effects of high pressure and high temperature on some physical properties of oceanic sediments, *J. Geophys. Res., 89*, 511-526, 1984.

Morton, J., and N. Sleep, A mid-ocean ridge thermal model, constraints on the volume of axial hydrothermal heat flux, *J. Geophys. Res., 90*, 11,345-11,353, 1985.

Mottl., M. J., Hydrothermal convection, reaction and diffucion in sediments on the Costa Rica Rift flank, pore water evidence from ODP sites 677 and 678, *Proceedings of ODP Scientific Results*, vol. 111, Ocean Drilling Program, College Station, TX, in press, 1989.

Mottl, M., J. Lawrence, and L. Kergwin, Elemental and stable isotopic composition of pore waters in carbonate sediments from Deep Sea Drilling sites 501/504 and 505, *Initial Reports Deep Sea Drill. Proj., 69*, 461-473, 1983*a*.

Mottl, M., E. R. M. Druffel, S. R. Hart, J. R. Lawrence, and E. S. Saltzman, Chemistry of hot waters sampled from basaltic basement in hole 504B, Deep Sea Drilling Project leg 83, Costa Rica Rift, *Initial Reports Deep Sea Drill. Proj., 83*, 315-328, 1985.

Mottl, M., R. N. Anderson, W. J. Jenkins and J. R. Lawrence, Chemistry of waters sampled from basaltic basement in Deep Sea Drilling Project holes 501, 504B and 505B, *Initial Reports Deep Sea Drill. Proj., 69*, 474-484, 1983*b*.

Narasimhan, T. N. and P. A. Witherspoon, An integrated finite difference method for analyzing fluid flow in porous media, *Water Resour. Res., 14*, 416-428, 1976.

Nield, D. A, Onset of thermohaline convection in a porous medium, *Water Resour. Res., 4*, 553-560, 1968.

Noel, M., Heat flow, sediment faulting and porewater advection in the Madiera Abyssal Plain, *Earth Planet. Sci. Lett., 73*, 398-406, 1985.

Noel, M., and M. W. Hounslow, Heat flow evidence for hydrothermal convection in Cretaceous crust of the Madiera Abyssal Plain, *Earth. Planet. Sci. Lett., 90*, 77-86, 1988.

Parsons, B., and J. G. Sclater, An analysis of the variation of ocean floor bathymetry and heat flow with age, *J. Geophys. Res., 82*, 803-829, 1977.

Sancetta, C. A., Biostratigraphic and paleoceanographic events in the eastern equatorial Pacific, results of Deep Sea Drilling Project leg 69, *Initial Reports Deep Sea Drill. Proj., 69*, 311-320, 1983.

Sayles, F. L., and W. J. Jenkins, Advection of pore fluids through sediments in the equatorial east Pacific, *Science, 217*, 245-248, 1982.

Sleep, N., and T. Wolery, Egress of hot water from mid ocean

ridge hydrothermal systems, some thermal constraints, *J. Geophys. Res., 83,* 5913-5922, 1978.

Spooner, E. T. C., and C. J. Bray, Hydrothermal fluids of seawater salinity in ophiolitic sulfide ore deposits in Cyprus, *Nature, 266,* 808-812, 1977.

Straus, J. M., Large amplitude convection in porous media, *J. Fluid Mech., 64,* 51-63, 1974.

Tsang, C.-F., and C. Doughty, Detailed validation of a liquid and heat flow code against field performance, *Rep. LBL-18833,* Lawrence Berkeley Laboratory, Berkeley, Calif., 1985.

Vanko, D. A., Temperature, pressure and composition of hydrothermal fluids,with their bearing on thef magnitude of tectonic uplift at mid-ocean ridges, inferred from fluid inclusions in oceanic layer 3 rocks, *J. Geophys. Res., 93,* 4595-4611, 1988.

Whitmarsh, R. B., Along-strike amplitude variations of oceanic magnetic stripes, are they related to low-temperature hydrothermal circulation?, *Geology, 10,* 461-465, 1982.

Wilkens, R. H. and M. G. Langseth, Physical properties of sediments of the Costa Rica Rift, Deep Sea Drilling Project sites 504 and 505, *Initial Reports Deep Sea Drill. Proj., 69* , 659-674, 1983.

Williams, C. F., T. N. Narasimhan, R . N. Anderson, M. D. Zoback and K. Becker, Convection in the oceanic crust, simulation of observations from Deep Sea Drilling Project hole 504B, Costa Rica Rift, *J. Geophys. Res., 91,* 4877-4889, 1986.

Williams, D. L., R. P. Von Herzen, J. G. Sclater and R. N. Anderson, The Galapagos Spreading Centre, lithospheric cooling and hydrothermal circulation, *Geophys. J. R. Astron. Soc., 38,* 587-608, 1974.

K. Becker, Division of Marine Geology and Geophysics, Rosenstiel School of Marine and Atmospheric Science, University of Miami, Miami, FL 33149.

A. T. Fisher, Ocean Drilling Program, Texas A & M University, 1000 Discovery Drive, College Station, TX 77840.

M. G. Langseth, Oceanography, Lamont-Doherty Geological Observatory, Palidsades, NY 10964.

M. J. Mottl, Hawaii Institute of Geophysics, University of Hawaii, 2525 Correa Road, Honolulu, HI 96822.

T. N. Narasimhan, Earth Sciences Division, Lawrence Berkeley Laboratory, Room 1106, Building 90, Berkeley, CA 94720.

(Received March 22, 1989;
revised July 20, 1989;
accepted June 11, 1989.)